ADVANCES IN INORGANIC CHEMISTRY, VOL. 38

EPR SPECTROSCOPY OF IRON–SULFUR PROTEINS

WILFRED R. HAGEN

Department of Biochemistry, Agricultural University, 6703 HA Wageningen, The Netherlands

I. Introduction

A. EPR Spectroscopy of Metalloproteins

The phenomenon of electron paramagnetic resonance (EPR) was discovered in 1945 (*1*) and was developed during the following decade by physicists into a practical method of spectroscopy. Initially, the objects of study were predominantly those of the solid-state physicist, i.e.,

defects in crystals with well-defined symmetry properties. As a consequence, the original experiments and theoretical developments were biased toward single-crystal systems and the optimal use of symmetry arguments and perturbation theory methods. This bias is reflected in the structure of the classical textbooks on EPR (e.g., Ref. *2*).

The first EPR experiments on biological systems were carried out very much along the same lines. In the mid-1950s, a group of physicists at Cambridge University, led by D. J. E. Ingram, made a series of single-crystal EPR studies on hemoglobin derivatives (*3, 4*). They took many spectra as a function of the orientation of the magnetic field with respect to the axes of the hemoglobin crystals frozen in their mother liquor. They were able to determine the orientation of the g-tensor principal axes with respect to crystal axis systems. Later, with the X-ray structures available, the g-tensor axes were found to approximately correspond to the heme plane and heme normal. The authors concluded that, "detailed information on the orientation of the haem plane can be combined with X-ray measurements to calculate the polypeptide chain directions and similar factors" (*4*).

In spite of the conceptual and experimental beauty of this work, in hindsight we can now assess single-crystal EPR to have proved to be of little value to protein structure determination. In fact, single-crystal EPR studies per se make up an extremely small part of all biological EPR work. This is not only the case because of the obvious practical difficulties of the protein crystallization and of the collection of angular-dependent data. There are also two fundamental difficulties intrinsic to the nature of proteins.

First, a biological metal site formally does not have any symmetry at all, if only because it is ligated by a polypeptide made up of levorotatory amino acid residues. This is especially true when the protein ligation forms a part of the first coordination sphere, as in iron–sulfur proteins. The statement implies that g-tensor axes cannot in general be expected to coincide with molecular bonds. Incidentally, it also explains why biochemists frequently run into problems when they attempt to analyze their EPR spectra using the high-symmetry approaches of the solid-state physicists.

Second, it so happens that the line width in single-crystal protein EPR is similar to (and frequently even significantly larger than) that of the turning-point features in spectra from randomly oriented samples of frozen solutions. There is no increased resolution in protein single-crystal spectra. This fact is related to the phenomenon of g strain that will be discussed later.

Also, in the mid-1950s, R. H. Sands studied transition ions in glasses

and he showed that the principal values of the g tensor and hyperfine tensors can be obtained from a single spectrum of a randomly oriented sample (*5*). The current widespread application of EPR spectroscopy to metalloproteins traces back to the late 1950s, when biochemist H. Beinert from the University of Wisconsin started to collaborate with physicist Sands at the University of Michigan and to apply the "powder EPR" method to frozen solutions of biological samples. Their first shot was at copper in cytochrome oxidase (*6*). A year later, in 1960, their second study was on mitochondrial membranes, in which they made the historical detection of what has long become an equivalence to iron–sulfur clusters, "the $g = 1.94$ signal" (*7, 8*). While the subsequent discussion about the physical and chemical nature of this signal spanned the better part of the ensuing decade, the detection itself is generally—perhaps with the exception of the authors themselves—felt to be the zero point in time of the history of iron–sulfur biochemistry. It is obviously also the first EPR experiment on an iron–sulfur cluster.

B. EPR Spectroscopy of Iron–Sulfur Proteins

The story of the genesis of iron–sulfur biochemistry from the observation of the $g = 1.94$ EPR signal is exemplary for all subsequent major developments in this field. The typical three-phase sequence of events is as follows. The first act is always the detection of an unusual, namely at the time unexplainable, EPR signal. This spurs a free flow of creative thinking, which one then attempts to contain and direct by collecting complementary information. Extensive analytical determinations, e.g., of Fe and acid-labile S content are a mandatory step, although these frequently prove to be rather less conclusive than one would want them to be. Of the other spectroscopies, Mössbauer usually provides a vital piece of the puzzle, notably, in the form of a ratio number of different iron sites, e.g., those with ferric over those with ferrous character. At this point then the time is ripe to formulate "the grand concept" that ties all loose ends together. In the final stage, corroboration is provided by, e.g., X-ray structural determinations, this making the system amenable to structure–function studies on a detailed level.

The assignment of the $g = 1.94$ line to an iron complex was initially controversial when the possibility of clustering of ions was not yet considered. The paramagnet should be high-spin ferric, which was known to exhibit extremely small (in the third decimal), and usually positive, deviations from the free-electron g value of 2.0023, as a consequence of what is known as effective quenching of orbital angular momentum for d^5 systems (*2*). Attempts to reconcile the incompatible

led to several instants of "creative theorization" (*9–12*). Also in the same period the idea was formulated of antiferromagnetic Heisenberg exchange coupling between an iron pair of unlike valence, together with the vector coupling model to derive effective g values (the g = 1.94 line) and hyperfine coupling values (*13, 14*). However, it was only several years later that this idea proved to be "the grand concept" for [2Fe–2S] clusters. It had first to be rejected by one of the original proposers (*12*), and subsequently found sufficient support in magnetic susceptibility (*15*), electron–nuclear double-resonance (ENDOR) (*16*), Mössbauer (*17*), and infrared (*18*) measurements to deserve reproposing on a sound experimental basis (*19*) and, later, theoretical elaboration (*20–25*; see Section II,B,3). This took place well into the 1970s and in the third and final historical phase, in which the concept of exchange coupling was extended to [4Fe–4S] clusters, and in which several X-ray structures were solved. Today these single-electron transferring Fe–S proteins form one of the best characterized classes of metalloproteins. A small caveat: our last statement does not always hold for the assignment of a specific biological role to soluble electron-transferring Fe–S proteins, and generally does not hold for the mechanism(s) of their biosynthesis.

There is a second class of Fe–S proteins whose members do not appear to be involved in net electron transfer at all, but rather act as complex Lewis acids (*26–28*). The chronicle of this class is very much that of the enzyme aconitase studied by Beinert and collaborators. This in its turn is an outgrowth of the discovery and identification of the 3Fe cluster, a sequence of events that bears remarkable similarity to the g = 1.94 story.

The 3Fe story evolves some one and one-half decades out of phase with the 2Fe story. It also starts with an unusual EPR signal, namely a relatively symmetrical and sharp one at g = 2.01. It was initially observed in membrane particles (*29, 30*), and membrane protein complexes (*31, 32*), and in a soluble protein from mitochondria (*33*) [which only several years later turned out to be identical to aconitase (*34*)]. Purification of the latter one allowed for the identification of the g = 2.01 signal with iron (*33*). Also, ^{57}Fe broadening was observed with bacterial membranes (*30*). For several years the signal was associated with the word HiPIP (high-potential iron protein), although at that time this acronym was already unambiguously assigned to the $[4Fe–4S]^{3+/2+}$ structure. This mix-up led to amusing misconceptions, such as the "low-potential HiPIP" (*35*). Although "soluble HiPIP" (i.e., aconitase) contained 3Fe per $S = \frac{1}{2}$ EPR signal, this stoichiometry was initially considered to be "not readily interpretable," because there

were only 2Fe per protein molecule (*36*). It was only when the Mössbauer spectroscopy of reduced ferredoxin I from *Azotobacter vinelandii* revealed the very characteristic, and not hitherto observed, 2 : 1 intensity pattern (*37*) that all pieces once more fell into place and thus allowed for the formulation of the grand concept, namely, of the existence of 3Fe clusters (*37*). This paved the way for a whole range of derived concepts, e.g., the [3Fe–4S] cluster structure (*38, 39*), cluster interconversions (*39–41*), localized valence states (*42, 43*), and the $[4Fe–4S]^{2+}$ Lewis acid (*42*). With some hop, step, and jump in the first X-ray analysis of a 3Fe protein (*44–46*), this story has come to a close. Today we have already entered a new period of detailed studies on the structure–function of both 3Fe proteins and $[4Fe–4S]^{2+}$ enzymes. Yet another caveat: the biological function of the 3Fe cluster remains controversial.

Add another one and one-half decades to the discovery of the "soluble HiPIP" (i.e., aconitase) signal to arrive at approximately the time of this writing. Is there room for yet another renaissance of iron–sulfur biochemistry, and if so, then where to look for it?

Several multicenter iron–sulfur proteins do not seem to fit the patterns outlined thus far. These complex proteins are usually enzymes; however, they are not of the nonredox, Lewis acid type. They are also not of the single-electron transferring type. The catalyzed redox reactions are nonradical wet chemistry, i.e., they involve the transfer of pairs, or multiple pairs, of electrons. The Fe–S content of these proteins is generally quite high.

As every new development in this field starts with an unusual EPR signal, so does this story. In this case a whole collection of unusual signals has been found in recent times: there are those with very high g values from very high-spin systems; there are also semiforbidden signals from high-integer spins, and there are the $S = \frac{1}{2}$ signals with all three g values below the free-electron value.

As this third wave in Fe–S history has only just started to unroll, we cannot perhaps yet be expected to recognize a unifying principle if we see one. Presently, it appears likely [at least to this author (*47–59*); see also Refs. *60–63*] that the "grand concept" for this class of Fe–S proteins will encompass the notion of "larger Fe–S structures," or "superclusters" (i.e., larger than 4Fe–S), and the notion of single-(super)cluster-based multiple-redox transitions. Whatever will crystallize out in its due time, already the current studies of these proteins have provided several novel types of biological EPR spectra ("superspins"; cf. Refs. *49, 51, 52, 54–57, 59, 63*), which will be discussed at length below. There is even a first indication of consolidation of the supercluster concept in

the form of x-ray crystallographic data on the P-clusters in nitrogenase (*64, 65*).

C. The ELS Classification

Classifications should be an aid in mastering complicated sets of data. In the official classification of iron–sulfur proteins (*66*), 3Fe clusters as well as mixed-metal clusters are not considered. The major distinction is between simple and complex iron–sulfur proteins. "Complex" is to indicate the presence of additional redox groups, e.g., flavin, molybdenum, and heme. The simple proteins are further subdivided into proteins containing one cluster and two clusters. This approach is not practical in simplifying a discussion of the EPR of iron–sulfur proteins.

In previous general reviews on Fe–S EPR, a common classification was according to the number of iron ions in a cluster, e.g., 1Fe, 2Fe, 3Fe, 4Fe, 2 × 4Fe (cf. Refs. *67–69*). These schemes are similarly less suited for our present purposes as we are in the course of reorienting our spectroscopy to also deal with problems other than the characterization of small Fe–S proteins. This reviewer has found some use in starting from a rather different choice of categories, and this he calls the "ELS classification": class E, *E*lectron transfer Fe–S proteins; class L, nonredox Fe–S enzymes that act as *L*ewis acids; and class S, putative *S*upercluster-containing Fe–S redox enzymes.

This is a classification based on biological function. It also corresponds to the three waves in the history of iron–sulfur proteins outlined above. From the point of view of the EPR spectroscopist, the three classes stand for three dissimilar experimental and theoretical objectives. The proteins of class E are well characterized. EPR is used on them either as a routine analytical measurement, or to support the development of sophisticated theory (cf. g strain; double exchange) by test measurements in which the proteins are no more than just model systems. The class L proteins are EPR silent in their active form; however, at least some of them can become paramagnetic upon chemical reduction. In this state they can be scrutinized by EPR—and more effectively by the derived technique of ENDOR—as an indirect way to learn about enzyme mechanisms (*27*). Class S proteins are the most complicated and the least defined structures. The spectroscopy now means making the first intrusions into an area of novel Fe–S arrangements and of unusual high-spin EPR signals. The concept of the ELS classification is summarized in Table I.

TABLE I

THE ELS CLASSIFICATION: SUMMARY OF THE CURRENT STATUS OF EPR SPECTROSCOPY OF IRON–SULFUR PROTEINS

Classification	Class E	Class L	Class S
Biological function	Single e^- transfer	Nonredox enzymes	Redox enzymes
First year (Ref.)	1960 (*7, 8*)	1978 (*34*)	1987 (*49*)
EPR theory	Advanced	Irrelevant	Developing
EPR application	Routine analysis	Indirect enzymological tool	Exploring
Typical spectrum	$g \approx 2.1$–1.8	None from native enzyme	Complex ($g \approx 18$–1)

II. Fundamentals of Iron–Sulfur EPR

A. THE BASIC BUILDING BLOCKS

Lemma i: the valency of each iron in Fe–S clusters is always III or II. The iron ion can exist in many valency states; however, the aqueous solution chemistry of iron complexes is essentially limited to the ferric and the ferrous states. The redox behavior of iron in proteins is presumably to a large extent a subset of this chemistry. The occurrence, if only transient, and perhaps even only formally, of higher oxidation states Fe(IV) and Fe(V) has been proposed for a few hemoproteins reactive toward molecular oxygen. Similar proposals have thus far never been put forth in relation with iron–sulfur structures. Considering the iron site in rubredoxins is probably as close as one can get in modeling the individual iron site in iron–sulfur clusters. The FeS_4 sites in rubredoxins (*70, 71*), desulforedoxin (*72*), and desulfoferrodoxin (*73*) all have a "garden variety" Fe^{3+}/Fe^{2+} reduction potential around 0 mV. The putative FeS_4 site in rubrerythrins has $E_m \approx +230$ mV (*74*).

Lemma ii: the spin state of each iron ion in Fe–S clusters is purely high spin. The d^5 ferric ion is high-spin $S = \frac{5}{2}$ or low-spin $S = \frac{1}{2}$; the d^6 ferrous ion is high-spin $S = 2$ or low-spin $S = 0$. Other possibilities are theoretically unfavorable and experimentally rare (cf. Ref. *75*). The six-coordinated iron in hemoproteins experiences a crystal field whose strength is of the order of the high-spin to low-spin cross-over energy. X-Ray crystallography on iron–sulfur proteins has thus far shown that

the crystal field around the iron is deformed tetrahedral. The crystal field splitting for tetrahedral coordination being only four-ninths that of the equivalent octahedral case implies that low-spin configurations are unlikely. Tetrahedrally coordinated mononuclear iron in proteins, e.g., rubredoxin (*76*), desulforedoxin (*72*), desulfoferrodoxin (*77*), rubrerythrin (*74*), and iron superoxide dismutase (*78*), is exclusively high spin. It is, therefore, to be expected that Fe–S clusters are made up only of ferric $S = \frac{5}{2}$ and/or ferrous $S = 2$ building blocks.

Note, however, that recent evidence suggests that higher iron coordination numbers are possible. One case is presented by the special iron in the cubane of aconitase, where binding of substrate leads to five, possibly six, coordination (*42*). Another, presently more remote, possibility is suggested by the structure of capped prismane model compounds, containing one or two six-coordinated metals capping the prismane core (*79*). In principle, the extension to six-coordinated iron in Fe–S proteins would make low-spin configurations possible. Rather strong-field ligands would, however, be required to add up with the weak-field sulfide contributions. A model system for this phenomenon has recently been synthesized (*80*).

Lemma iii: the bridging ligand in iron–sulfur clusters is μ-sulfide. This almost tautological statement excludes the Fe–(μ-O)–Fe dinuclear-type clusters (cf. Ref. *81*) from our present considerations. The μ–S^{2-} as a ligand to the iron ion is both consistent with the absence of higher Fe oxidation states and the absence of low-spin configurations.

It has been proved possible to do a chemical (i.e., as a treatment of purified protein) global replacement of the μ–S^{2-} in a few Fe–S proteins by μ–Se^{2-} with two interesting consequences for the EPR spectroscopist. First, note that both S^{2-} and Se^{2-} are soft Lewis bases, therefore ligands with potential covalent character. Thus, from the $[2Fe–2^{77}Se]^{1+}$-containing adrenal ferredoxin, ^{77}Se ($I = \frac{1}{2}$) splittings in the $S = \frac{1}{2}$ X-band EPR are readily observed as a consequence of delocalization of the spin onto the two bridging ligands. This was early support for the [2Fe–2X] structure (*82*). Second, the ionic radius of Se^{2-} is significantly greater than that of S^{2-}; the S → Se substitution means an increased strain on the protein fold. The 2 $[4Fe–4Se]^{1+}$ configuration in *Clostridium pasteurianum* ferredoxin was the first example of a spin mixture and also of the system spin $S = \frac{7}{2}$ in an iron–"sulfur" protein (*83, 84*). Note, however, that the acid-labile S/Se substitution has not been shown to be, nor is it expected to be, of any biological relevance.

Lemma iv: the external ligation of iron–sulfur clusters is (predominantly) by the cysteine thiolate side group. This is rather a statement to be questioned. Mixed ligation by sulfur and nitrogen, $(Cys)_2(His)_2$, of

the [2Fe–2S] cluster in the Rieske protein appears to be well established (*85–88*). Mixed ligation by sulfur and oxygen, $(Cys)_3(Asp)$, has been proposed for one of the [4Fe–4S] clusters in *Desulfovibrio africanus* ferredoxin III (*89, 90*) and for the single cubane in *Pyrococcus furiosus* ferredoxin (*91*). Partial ligation by nitrogen has been inferred from frequency-dependent line broadening in the EPR of a putative prismane [6Fe–6S]-containing protein from *Desulfovibrio vulgaris* (*59*). However, in most, if not all, cases, the Cys ligation is at least 50%, and for the majority of thus-far scrutinized systems it is, in fact, 100%. In other words, lemma iv is a statement about the relative lack of variation in the external ligation of Fe–S clusters.

> Proposition: the building blocks of iron–sulfur structures are very limited in number; therefore, the possible Fe–S structures are limited in number; therefore, the great variation in magnetic and redox properties is imposed by the higher coordination spheres, i.e., the protein and the solvent, and—if there is one—by the substrate.

This statement summarizes the previous four lemmae and points to their implications for the EPR spectroscopist. There are simply four building blocks to construct biological Fe–S clusters from. These are the high-spin ferric ion, the high-spin ferrous ion, the μ-sulfide ion, and the cysteinate side group (with a limited possibility to replace the latter by one or two other amino acid residues). These four elements should provide the structural/chemical basis to explain the basic features of iron–sulfur protein EPR. What remains then are the variations in these EPR features and any additional unexplained properties. These remainders are really the raisins in the pudding, as they represent (bio)chemically relevant information in addition to a simple cluster identification. However, we have only just begun to explore these fields. At this point in time, progress in dealing with the details of Fe–S EPR is still limited even for the best characterized class T electron transfer iron–sulfur proteins. We come back to this theme when we discuss *g* strain.

B. SUPEREXCHANGE

1. Heisenberg Exchange Interaction

When two paramagnetic ions are close to each other they can be subject to direct Heisenberg exchange interaction. This quantum mechanical phenomenon comes about by a finite overlap of the symmetry-adapted molecular orbitals of the individual metal centers. It effectively

results in a decreased energy for the ground state of the coupled complex. The interaction of two local spins $\mathbf{S}_1$ and $\mathbf{S}_2$ is described by the Hamiltonian:

$$H_{\text{exchange}} = J\mathbf{S}_1 \cdot \mathbf{S}_2 \qquad \text{(plus higher order terms)} \tag{1}$$

This direct interaction is *not* operative in Fe–S clusters; there is no direct metal–metal bond. The coupling is via the μ-bridging sulfides, therefore, it is termed indirect exchange or superexchange. This anisotropic interaction is commonly described (cf. Ref. *2*, p. 495) with the Hamiltonian:

$$H_{\text{superexchange}} = J\mathbf{S}_1 \cdot \mathbf{S}_2 + \mathbf{S}_1 \cdot \mathbf{K} \cdot \mathbf{S}_2 + \mathbf{Q} \cdot (\mathbf{S}_1 \times \mathbf{S}_2) \tag{2}$$

The three terms describe the isotropic, the anisotropic, and the asymmetric part of the exchange, respectively. J is a scalar, $\mathbf{K}$ is a symmetric tensor, and $\mathbf{Q}$ is an antisymmetric tensor. The latter two terms are not easily dealt with especially in noncrystalline material. In relation to Fe–S clusters they have been thus far ignored, and we have presently no choice but to continue to adhere to this—silently made—assumption. Thus, the Heisenberg exchange interaction in Fe–S clusters is described by an effective Hamiltonian:

$$H_{\text{superexchange}} \approx J'\mathbf{S}_1 \cdot \mathbf{S}_2 \tag{3}$$

This describes the angular average of Eq. (2). In practice, the prime is dropped from J'.

The far-reaching consequences of the Heisenberg exchange interaction for the EPR of Fe–S clusters is readily illustrated on the simplest possible example, the one-electron reduced $[2\text{Fe–2S}]^{1+}$ cluster. Mössbauer spectroscopy indicates that the "excess electron" is essentially localized on one of the two iron ions (*17*), i.e., we have well-defined high-spin ferric and high-spin ferrous entities. This is a simple example for which the epitaph "localized valence" (*92*) has in recent years become generally accepted. EPR spectroscopy, however, does not show the expected $S = \frac{5}{2}$ and $S = 2$ spin systems, but rather reveals one single $S = \frac{1}{2}$ spectrum per reduced [2Fe–2S] cluster. Thus, the two spin systems have been "strongly," antiferromagnetically coupled into a single, new paramagnet with a ground state effectively described as carrying a spin $S = \frac{1}{2}$.

2. *The Gibson Model*

The first model to successfully describe this situation in a semiquantitative manner is the previously mentioned Gibson model (*13, 14*). In this antiferromagnetic-coupling model Gibson *et al.* make the following

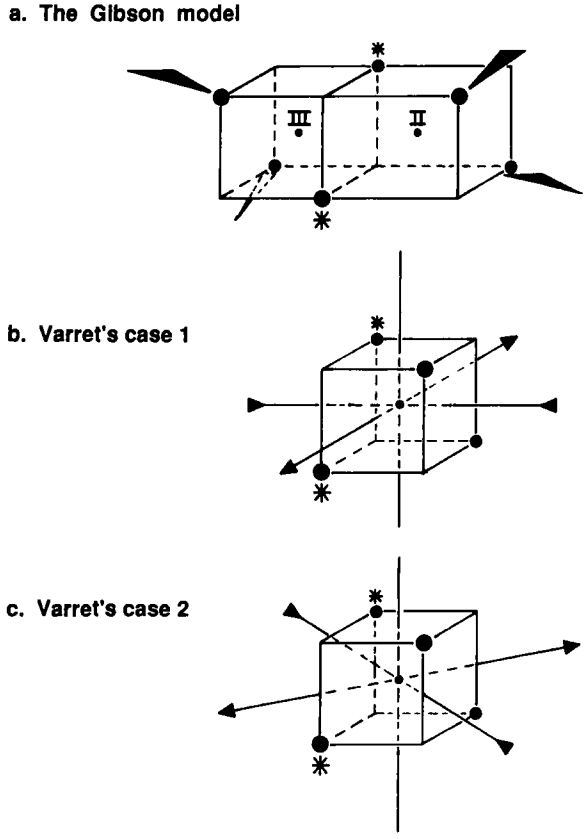

FIG. 1. Distortion of the ferrous site in dinuclear clusters under the Gibson model (a) or the Bertrand–Gayda model (b or c). An asterisk indicates acid-labile sulfide.

assumptions (or symmetry simplifications): (1) the symmetry at the ferric site is tetragonal; (2) the symmetry at the ferrous site is tetrahedral. Graphically this situation can be represented as in Fig. 1a by Fe^{3+} in a cube and Fe^{2+} in an adjacent cube elongated along the Fe–Fe axis. For EPR this means (1) the g tensor of the Fe^{3+} ion is isotropic, its scalar value being slightly greater than g_e; (2) the Fe^{2+} g tensor has its z axis colinear with the Fe–Fe axis, and $g_z = g_e$.

Making these two assumptions, and assuming the Hamiltonian Eq. (3) to hold, and with the usual procedure of angular momentum projection operators,

$$g_{\text{dimer}} = c_1 g_1 + c_2 g_2 \tag{4a}$$

$$c_1 = [S(S + 1) + S_1(S_1 + 1) - S_2(S_2 + 1)]/2S(S + 1) \quad (4b)$$

$$c_2 = [S(S + 1) + S_2(S_2 + 1) - S_1(S_1 + 1)]/2S(S + 1) \quad (4c)$$

one readily obtains the Gibson model g-tensor equations for the effective g tensor of the $S = \frac{1}{2}$ ground state:

$$g_{x\text{-dimer}} = (\tfrac{7}{3})g_{x\text{-ferric}} - (\tfrac{4}{3})g_{x\text{-ferrous}} \quad (5a)$$

$$g_{y\text{-dimer}} = (\tfrac{7}{3})g_{y\text{-ferric}} - (\tfrac{4}{3})g_{y\text{-ferrous}} \quad (5b)$$

$$g_{z\text{-dimer}} = (\tfrac{7}{3})g_{z\text{-ferric}} - (\tfrac{4}{3})g_e \quad (5c)$$

For the ferric g tensor, Gibson *et al.* take the isotropic value $g = 2.019$ (from Fe^{3+} in ZnS). The sixth electron of the ferrous ion is taken to be in the $|z^2\rangle$ orbital; therefore, assuming local tetragonal symmetry, the ferrous g tensor is

$$g_{x\text{-ferrous}} = g_e + 6\lambda/\Delta_{yz} \quad (6a)$$

$$g_{y\text{-ferrous}} = g_e + 6\lambda/\Delta_{zx} \quad (6b)$$

$$g_{z\text{-ferrous}} = g_e \quad (6c)$$

The quantity Δ_{ij} is the crystal field splitting between the $|z^2\rangle$ single-electron ground state and the excited state $|ij\rangle$.

The strength of this model is in its prediction that two of the g values are significantly below g_e (i.e., in its explanation of "the" $g = 1.94$ EPR signal) and that the third g value is greater than g_e. All thus far reported EPR spectra on $[2Fe\text{–}2S]^{1+}$ structures are consistent with this model (specifically, cf. Ref. *93*).

3. *The Bertrand–Gayda Model*

The symmetry assumptions of the Gibson model are of course unrealistic for protein Fe–S sites. Bertrand and Gayda have elaborated on the model by relaxing some of the high-symmetry restrictions (*20*). The crux of the Bertrand–Gayda model is to make the EPR observables (e.g., effective g values) a function of the rhombicity at the ferrous site expressed in terms of a single parameter, Θ. This latter concept comes from the work of Varret on high-spin ferrous ions (*94*). Varret defines two possible ways of rhombically distorting a tetrahedral site, and these are depicted in Fig. 1.

The Bertrand–Gayda model differs from the Gibson model in two aspects. It allows for rhombicity at the ferrous site, assuming Varret's "case 2" (cf. Fig. 1c) to be operative. It also allows for a rhombic g tensor from the ferric ion, however, without attempting to specify its source

or to model its physics. Furthermore, the two g tensors are assumed to be colinear in order to retain the validity of the coupling Eqs. (4a)–(4c).

Just as the Gibson model is a crystal field approach, so is the Bertrand–Gayda model. It starts from the metal d orbitals in a tetragonal field and then mixes these as a result of rhombic deformation in c_{2v} symmetry. The lowest one-electron orbital (i.e., the one containing the sixth electron) is now

$$|\phi_0\rangle = \cos\Theta\,|z^2\rangle + \sin\Theta\,|x^2 - y^2\rangle \tag{7}$$

in which Θ measures the mixing of the $|z^2\rangle$ and $|x^2 - y^2\rangle$ states and also reflects some "degree" of rhombicity. The expressions for the ferrous g-tensor values now become

$$g_{x\text{-ferrous}} = g_e + (8\lambda/\Delta_{yz})\sin^2(\Theta + \pi/3) \tag{8a}$$

$$g_{y\text{-ferrous}} = g_e + (8\lambda/\Delta_{xz})\sin^2(\Theta - \pi/3) \tag{8b}$$

$$g_{z\text{-ferrous}} = g_e + (8\lambda/\Delta_{xy})\sin^2\Theta \tag{8c}$$

and the effective g values for the cluster are again calculated with Eqs. (5a)–(5c). Note that Eqs. (8a)–(8c) reduce to Eqs. (6a)–(6c) for $\Theta = 0$. A sign error in the original equations was corrected by Hearshen *et al.* (*25*); the above equations are the corrected ones. Also, they are valid for both types of distortion discerned by Varret (cf. Fig. 1, b and c).

Bertrand *et al.* have used the Bertrand–Gayda model as a means for systematic research on structural variations in dinuclear clusters (*20–23*). In order to comply to the format used in an early phenomenological study (*95*), the authors cast their analyses in the form (which they call the Coffman representation) of plots of the three clusters g values, g_x, g_y, and g_z, versus an unnamed, phenomenological parameter χ, defined as

$$\chi = g_y - g_x \tag{9}$$

It should be noted (in the opinion of the present reviewer) that this Coffman representation is only one out of an infinite number of possible ways to graphically analyze the EPR data, and it is not necessarily the most useful one. From Eqs. (5) and (8) it can be seen that the cluster g values are a function of the eight parameters g_{1x}, g_{1y}, g_{1z}, λ, Δ_{yz}, Δ_{xz}, Δ_{xy}, and Θ. By giving the first six of these parameters a fixed value, Bertrand *et al.* force the cluster g values to become a function of the latter two only. This has the practical advantage that two of the g values are a function of χ only, and also that for small values of Θ there is an almost linear relationship between χ and Θ. A disadvantage is that this form of the model is bound to prove its own premise, namely,

that structural variation in [2Fe–2S] clusters is a function of χ and Δ_{xy} only.

Some criticism has been ventured by Hearshen *et al.*, notably, on the use of a single set of ferric g values, where there is some evidence that the ferric ion in these systems can have large rhombic components, which are further "amplified" by the factor of $(\frac{7}{3})$ in Eqs. (5a)–(5c) (*25*). The authors also express concern over the fact that their analyses of g strain (see below) in ferredoxins indicate an inherent error in the experimental g values when identified with turning points in the powder spectrum (*25*). Bertrand *et al.*, however, are not convinced of the relevance of this latter error at the present state of accuracy in testing the model (*23*).

Finally, we note that even the assumption of C_{2v} symmetry at the ferrous site is a simplification of the real structure determined by X-ray crystallography (*96*).

C. Double Exchange

1. Valence Delocalization

When we reduce an $[2Fe–2S]^{2+}$ cluster with one electron equivalent, where does this "excess electron" go to? Is it always captured by one and the same iron? In an early attempt to describe the cause of g strain, Hearshen *et al.* played with the idea that there is a comparable chance for the electron to go to Fe_A or to Fe_B, i.e., resulting in a physical mixture of the states (Fe_A^{2+}, Fe_B^{3+}) and (Fe_A^{3+}, Fe_B^{2+}) (*97*). A simple graphical representation of this situation would be a symmetrical, one-dimensional potential well for the excess electron along the Fe–Fe axis with an infinitely high barrier at half-way (Fig. 2a). As this concept found little experimental support, it was later rejected in favor of a g-strain version of the Bertrand–Gayda model (*25*).

The question was readdressed theoretically from a different angle by Noodleman and Baerends (*98*), who considered the possibility that the excess electron would be delocalized over the sites Fe_A and Fe_B. We could denote this "resonance" situation, perhaps somewhat simplistically, as $(Fe_A^{2.5+}, Fe_B^{2.5+})$. For a quantum mechanical description of the phenomenon of excess electron delocalization, the classical reference is the paper by Anderson and Hasegawa on double-exchange interaction (*99*). The potential well for the excess electron is now flat, between site A and site B (Fig. 2b). An important generality in this respect was pointed out some years ago by Middleton *et al.* in their Mössbauer studies on the considerably more complicated [4Fe–4S] system: "Any

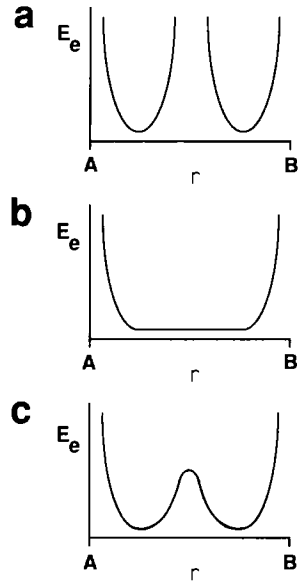

FIG. 2. Schematic representation of the potential of the excess electron (E_e) in an Fe_AFe_B cluster at a distance r from Fe_A when the iron valences (III/II) are fully localized (a), fully delocalized (b), or intermediate (c).

sharing of the electrons between the spin-up and the spin-down iron atoms is inhibited by the Pauli exclusion principle" (*100*). Noodleman and Baerends have again pointed to this generality, whose importance is not to be underestimated [here, we quote yet a later formulation by Day *et al.* (*101*)]: "Localized sites couple antiferromagnetically to produce the lowest spin system. On the other hand, sites which share a delocalized electron are coupled ferromagnetically to produce the highest system spin."

For the $[2Fe–2S]^{1+}$ cluster this means that, when the excess electron is localized at one of the iron ions, then the system spin for the ground state (i.e., the state observed by EPR at cryogenic temperatures) is $S_{dimer} = \frac{5}{2} - 2 = \frac{1}{2}$; when the excess electron is delocalized over the two iron sites, then the ground state has $S_{dimer} = \frac{5}{2} + 2 = \frac{9}{2}$. We have already seen that Mössbauer spectroscopy identifies the excess electron in [2Fe–2S] ferredoxins as being localized, and this is consistent with the $S = \frac{1}{2}$ ground state observed in EPR. Therefore, the mechanism of double exchange, or of charge delocalization, is probably not significant for the description of the ground state properties of these proteins

[although it may be relevant to the description of the highest state(s) of the spin ladder (*98*)]. Interestingly, dinuclear Fe(III/II) model compounds with bridging oxygens have recently been described and have been found to exhibit Mössbauer, EPR, and susceptibility properties consistent with a ground state system spin $S = \frac{9}{2}$ (*102–104*).

The present interest in double-exchange interactions has been spurred by the observation of valence delocalization in trimeric, cubane, and, possibly, superclusters. Mössbauer data on the $[3Fe–4S]^0$ cluster in inactive aconitase and in certain reduced ferredoxins (cf. Ref. *105* and references quoted therein) point to a situation in which one of the irons is localized high-spin ferric while the other two form a fully delocalized pair, i.e., $[(Fe_A^{2.5+}, Fe_B^{2.5+}), Fe_C^{3+}]$. Münck and Kent suggested that the spin of the internal (Fe_A, Fe_B) dimer is $S = \frac{9}{2}$ as a result of double exchange being the dominant interaction (*106*). The $S = \frac{9}{2}$ spin is then envisioned to couple antiferromagnetically to the $S = \frac{5}{2}$ spin of Fe_C, resulting in a system spin $S_{trimer} = 2$, consistent with, e.g., EPR data (*105, 107*).

This conceptually simple scheme was put to the test by Papaefthymiou *et al.*, who calculated ^{57}Fe hyperfine values under this model for the two "sites" (Fe_A, Fe_B) and Fe_C and compared these to their Mössbauer data on *D. gigas* ferredoxin II (*105*). The sign and magnitude of the predicted and experimental (angular-averaged) A values were found to be in very good agreement. Note, however, that the calculation involved some educated guesses on the starting A values for mononuclear ferric and ferrous sites from available literature data (*105*). We will not pursue this point here, but rather attempt a qualitative evaluation of the status quo of ongoing attempts to apply the concept of double-exchange interaction to understand the magnetic properties of iron–sulfur proteins. We are particularly interested in their relevance to EPR properties.

2. *Spin Ladders*

First, we have to point out that there is a mix-up of symbols in the literature for the Heisenberg part of the exchange interaction. Equation (3) can be found under three different forms:

$$H = -2J\mathbf{S}_1 \cdot \mathbf{S}_2 \tag{10a}$$

$$H = -J\mathbf{S}_1 \cdot \mathbf{S}_2 \tag{10b}$$

$$H = J\mathbf{S}_1 \cdot \mathbf{S}_2 \tag{10c}$$

The first form, Eq. (10a), was used in the early work on ferredoxins by Dunham and Sands and co-workers (*15, 19, 108*). This form has re-

mained in use in the Fe–S field up to today, specifically, in studies on bulk magnetic susceptibility (*101*). Note that under this form the quantity J has a negative value for $[2Fe–2S]^{2+/1+}$ clusters. The second form, Eq. (10b), was recently used by Ding *et al.* in their work on the dinuclear Fe model compound with $S = \frac{9}{2}$ ground state properties (*104*). The third form, Eq. (10c), has been used in all the recent work on double exchange in iron–sulfur structures, starting with the Noodleman–Baerends paper (*98*). Not without reluctance I follow here their convention. The reader is urged to check carefully what is the personal preference of each author in order to allow for a meaningful comparison of reported values (and signs!) of J.

With the Heisenberg-type superexchange between two metal sites, site A and site B, written as Eq. (10c), we have a spin ladder of states with absolute energies,

$$E(S_A, S_B, S_{AB}) = (J/2)\,[S_{AB}(S_{AB} + 1) - S_A(S_A + 1) - S_B(S_B + 1)] \tag{11}$$

in which S_A and S_B are the spin of the individual sites and S_{AB} is the system spin. The last two terms in Eq. (11) are a constant and since one is usually only interested in relative energies, the terms are simply dropped:

$$E(S_{AB}) = (J/2)[S_{AB}(S_{AB} + 1)] \tag{12}$$

With a positive value of J [that is, negative under the format of Eq. (10a) or (10b)] for a high-spin ferric–ferrous pair, we have the spin ladder given in Fig. 3A. When the metal pair is also subject to double-exchange interaction, a second term appears in the spin ladder equation:

$$E(S_{AB}) = (J/2)[S_{AB}(S_{AB} + 1)] \pm B(S_{AB} + \tfrac{1}{2}) \tag{13}$$

The term results from the double-exchange Hamiltonian (*98, 99, 104, 105, 109*):

$$H_{\text{double exchange}} = BV_{AB}T_{AB} \tag{14}$$

This operator works on the localized-valence dimer states $|A\rangle$ and $|B\rangle$ (where $|A\rangle$ means that the excess electron is on the A site, i.e., Fe_A^{2+}, Fe_B^{3+}) according to:

$$V_{AB}T_{AB}\,|B\rangle = V_{AB}\,|A\rangle = (S_{AB} + \tfrac{1}{2})\,|A\rangle \tag{15}$$

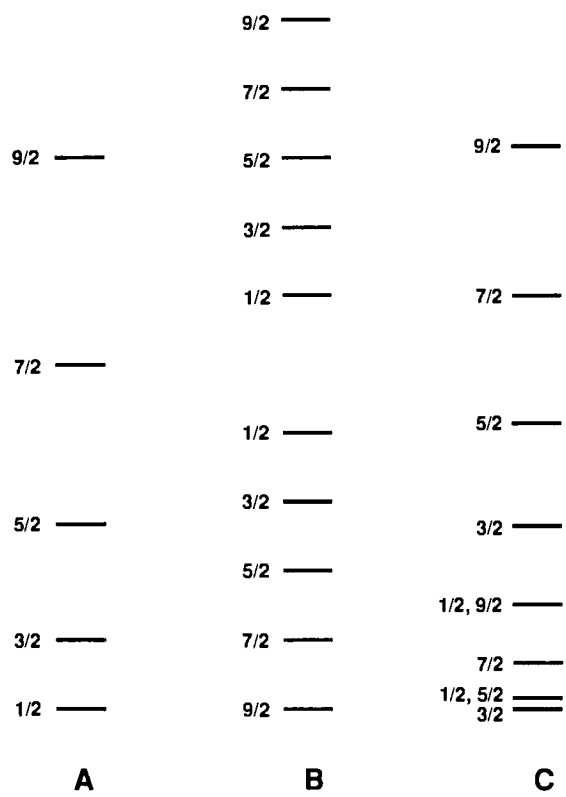

FIG. 3. Spin ladder of the dinuclear Fe(III/II) cluster subject to superexchange and double exchange with $J \gg B$ (ladder A), $J \ll B$ (ladder B), or $J = B/2$ (ladder C). The three ladders are not normalized to the same energy scale.

V_{AB} is a shift operator (sometimes called the double-exchange operator; cf. Ref. *104*), T_{AB} is a transfer operator, and the coefficient B in Eq. (14) is a transfer integral.

In simple words these equations have the following meaning: we start from the assumption that there exist two energetically degenerate states, $|A\rangle$ and $|B\rangle$, or (Fe_A^{2+}, Fe_B^{3+}) and (Fe_A^{3+}, Fe_B^{2+}). The $|A\rangle$ state is 100% occupied, the $|B\rangle$ state is empty. The effect of the $H_{\text{double exchange}}$ operator is twofold. It delocalizes the electron over the two sites, and it lifts the degeneracy of the two energy states.

Three typical situations can now occur. When $J \gg B$ then the excess electron is essentially localized. The potential well is as in Fig. 2a, and the spin ladder is as in Fig. 3A. The low-temperature EPR is that of an $S = \frac{1}{2}$ system. When $J \ll B$, then the excess electron is essentially fully

delocalized. The potential well is given in Fig. 2b, and the spin ladder is that of Fig. 3B. The low-temperature EPR should be characteristic of an $S = \frac{9}{2}$ system. A third possibility would be $J \approx B$. The energy barrier between the metals has a finite height (Fig. 2c). The spin ladder has an irregular, nested pattern (Fig. 3C). The EPR will be very sensitive to the value of J/B. For example, for the case of $2J = B$ (see Fig. 3C), the ground state is $S = \frac{3}{2}$ and there are two low-lying excited states with $S = \frac{1}{2}$ and $S = \frac{5}{2}$, respectively.

We anticipate that in the coming years the concept of double exchange will be a central theme in the more physically oriented studies on iron–sulfur proteins. The development is presently in its early phase, and this may bring along the risk of zealotry. It is, therefore, important that we realize the limitations as they stand, both in the theory and in the applications, and that we form a clear picture of what we want the ultimate goals of these efforts to be. First we consider the theoretical limitations.

3. *Double Exchange Evaluated*

The simple form in which we have outlined the theory is approximately the form in which it has thus far been applied to iron–sulfur structures. Under this form the two localized-valence configurations (Fe_A^{2+}, Fe_B^{3+}) and (Fe_A^{3+}, Fe_B^{2+}) are assumed to be fully equivalent; however, at the same time, the initial occupancy (i.e., before the application of the double-exchange operator) is assumed to be 100% biased toward the configuration with the ferrous form at the A site. The possibility of a "fractional occupancy" (i.e., a finite number of the molecules have ferrous at the B site) has not been considered since the early proposal by Hearshen *et al.* (*97*). The possibility of "intermediate cases" ($J \approx B$), resulting in level crossings, has only been touched upon (*104*). Is our simple picture of a finite, symmetrical barrier in a potential well meaningful? The situation in which the excess electron delocalizes over more than two sites is expected to lead to additional complications (*109*).

We now consider the applications per cluster type. The calculations of Noodleman and Baerends suggest that double exchange in oxidized and reduced [2Fe–2S] clusters is only significant when considering the highest levels of the spin ladder (*98*), and this is consistent with all EPR results thus far (i.e., $S = 0$, and $S = \frac{1}{2}$, for the ground states) as well as all other magnetic measurements, including those on bulk susceptibility (*15*).

For the oxidized $[3Fe–4S]^{1+}$ cluster, initially a model of isotropic, antiferromagnetic Heisenberg exchange between the three $S = \frac{5}{2}$ spins was proposed (*110, 111*). Two $S = \frac{5}{2}$ spins are coupled to an intermediate

spin $S' = 2$ (or 3), and this in turn is coupled to the third $S = \frac{5}{2}$ to yield the system spin of the trimer, $S = \frac{1}{2}$. This model appears to have stood the test of time remarkably well (*112–116*). It is consistent with the $S = \frac{1}{2}$ EPR now observed in innumerable cases as well as with other magnetic measurements, specifically a recent one on susceptibility (*101*). Double exchange has not been considered, as there is apparently no need to. A similar situation exists in the linear $[3Fe–4S]^{1+}$ cluster in "purple" aconitase, except that $S' = 5$ and the system spin is $S = \frac{5}{2}$ (*41*). Again, double exchange appears to be insignificant.

The reduced $[3Fe–4S]^{0}$ cluster has $S = 2$ EPR, and we have already seen that this is consistent with a model in which a (formally) ferric–ferrous pair forms a delocalized pair by strong double exchange resulting in $S' = \frac{9}{2}$. This in turn is coupled to the $S = \frac{5}{2}$ spin of the third iron to yield the system spin $S = 2$. The model has been tested by comparing calculated iron hyperfine splitting parameters with Mössbauer data on *D. gigas* ferredoxin II (*105*). There is some indication that the $[3Fe–4S]^{0}$ cluster in this protein has a low-lying excited state in which the electron is delocalized over all three Fe ions (*105*); however, it is presently not obvious how to interpret this data (*101, 109*).

The situation for cubane clusters is far less clear. Presently, the point of reference appears to be the idea that the iron in these clusters can be considered to occur in coupled pairs. This concept comes from the early Mössbauer studies of the Liverpool group on *Chromatium vinosum* HiPIP (*117–119*) and on *Bacillus stearothermophilus* ferredoxin (*100*). The proposals of these authors are summarized in the following scheme:

$[4Fe–4S]^{3+}$ is $(Fe^{3+}–Fe^{3+})$ coupled to $(Fe^{3+}–Fe^{2+})$
$[4Fe–4S]^{2+}$ is $(Fe^{3+}–Fe^{2+})$ coupled to $(Fe^{3+}–Fe^{2+})$
$[4Fe–4S]^{1+}$ is $(Fe^{2+}–Fe^{2+})$ coupled to $(Fe^{3+}–Fe^{2+})$

Within each pair the spins are coupled parallel, and the resulting dimer spins are coupled antiparallel to yield the cubane cluster spin. For all mixed-valence $(Fe^{3+}–Fe^{2+})$ pairs, an ad hoc delocalization is then assumed in order to explain Mössbauer indistinguishability of individual iron atoms. Indeed, this simple addition/subtraction of $S = \frac{5}{2}$ (ferric) and $S = 2$ (ferrous) spins leads to the ground state system spins of $S = \frac{1}{2}$, 0, and $\frac{1}{2}$, respectively, as we observe them, e.g., in EPR. Based on this scheme the authors even proposed a 4Fe version of the Gibson model in order to explain that HiPIP has $g > g_e$ (*119*), and ferredoxin has $g < g_e$ (*100*). The authors hasten, however, to state that the system is a complicated one and that the model should be looked upon as an

intermediate in a developing description. We do comply with this and refer the interested reader to the original papers (*100, 119*).

The relevance of the Liverpool model in the present context is that it has recently been revived by Noodleman in a form in which double exchange is considered explicitly, i.e., as the delocalization mechanism for the (Fe^{3+}–Fe^{2+}) pair in the $[4Fe–4S]^{3+}$ HiPIP-type core (*120*). Jordanov *et al.* have subsequently applied the model to analyze bulk susceptibility data from an $[Fe_4S_4(SR)_4]^{1-}$ complex, and they conclude it to be superior to a Heisenberg exchange-only model (*121*). Very recently, the model has also been considered as a basis to explain paramagnetic shifts in ^1H NMR from cysteine β-protons in HiPIPs (*122, 123*). The reviewer considers it too early to evaluate these results, and this especially so since he is presently involved in a project to redetermine the magnetic properties of HiPIP proteins. Two significant results of this work thus far are (1) the refutation of the long-standing Antanaitis–Moss model (*124*) for the EPR from *C. vinosum* HiPIP (and, therefore, a refutation of support from EPR data for the Liverpool model) and (2) the detection of four separate (instead of two pairs of) quadrupole doublets by high-resolution Mössbauer spectroscopy (*125*).

The relevance of double-exchange interaction to the explanation of the magnetic properties of the other two redox states of the cubane cluster in proteins—$[4Fe–4S]^{2+}$; $S = 0$, $[4Fe–4S]^{1+}$; $S = \frac{1}{2}$—has thus far not been tested experimentally in any way. An interesting aspect is the substrate-induced localized valence in aconitase (*42*).

In recent times, $S > \frac{5}{2}$ EPR has been reported for several iron–sulfur proteins, and evidence has been put forth to suggest that this is typically associated with clusters containing more than four ions (*49–59*). A cluster spin with a value larger than that of the high-spin ferric ion implies some sort of parallel spin coupling, i.e., suggestive of double-exchange interaction of significance. Although this possibility has thus far not been discussed, let alone tested experimentally, it is to be expected that the presently evolving research trends in double-exchange interactions and in superclusters/superspins will intertwine in the not too distant future.

In summarizing the previous paragraphs we note that there is reason to believe that the concept of double exchange is an essential element in the description of the magnetic properties of iron–sulfur clusters. Possible exceptions are the reduced 2Fe cluster and the oxidized 2Fe and 3Fe clusters (and perhaps all fully oxidized *n*Fe clusters). From an EPR spectroscopist's point of view the concept is especially important for the systems that have a ground state superspin, whose explanation requires some form of parallel spin alignment. At the same time we

should caution that any serious testing has thus far been limited to only one case, now several years ago, of a single protein (*105*).

Is there any added value for the biochemist in this tedious biophysics? When we know what the basic elements of iron–sulfur clusters are, we can understand the gross features of their EPR spectra. It is then from the fine details of these spectra that we can extract information specific for the protein at hand. Double exchange does not necessarily have *any* direct relevance to biology; however, with elements such as the $(Fe_A^{2.5+}–Fe_B^{2.5+})$ delocalized dimer we may be able to extend our list of basic building blocks beyond the four defined previously.

Perhaps a helpful way to look at this problem is to draw an analogy with the definition of structure levels in protein chemistry: the first four building blocks (cf. Section II,A.) are the basis of the primary magnetic structure of the iron–sulfur cluster; there is a secondary level of structure in the delocalized dimers, trimers, etc. within the cluster; a tertiary structural level is imposed on the cluster by the coordinating protein and its environment. All this contributes to the shape of the EPR spectrum. Thus, by a judicious definition of these structural elements and by an establishing of their contributions to the spectrum, we can improve on our capacities to sort out the general from the specific spectral features, i.e., the common from the detailed (bio)chemical information. These details are the subject of the following section.

III. *g* Strain in Doublet Systems

A. Inhomogeneous Broadening of Iron–Sulfur EPR

We now turn our attention to an "advanced" topic in the EPR of metalloproteins: *g* strain. The theory has been developed to a large extent with reference to well-characterized iron–sulfur proteins, i.e., to class E systems. I have recently reviewed the complete literature on *g* strain in metalloproteins (*126*). The present section is an updated summary of Ref. *126*.

The EPR of simple $S = \frac{1}{2}$ systems is described by the spin Hamiltonian:

$$H = \beta \mathbf{B} \cdot \mathbf{g} \cdot \mathbf{S} \tag{16}$$

This description should be valid for the low-temperature EPR of many iron–sulfur systems, as they have an $S = \frac{1}{2}$ ground state well separated from the other levels of their spin ladder. We assume here that the cluster under consideration is not subject to dipolar interaction, i.e., it

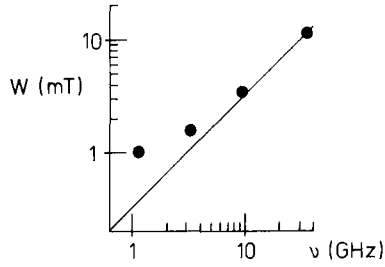

FIG. 4. The EPR line width of $[2Fe–2S]^{1+}$ in spinach ferredoxin as a function of the microwave frequency (from Ref. *126*).

is magnetically well isolated by the surrounding diamagnetic protein. This is, e.g., a valid assumption for proteins that contain only a single cluster (or only a single paramagnetic cluster). Note, however, that it is very difficult to avoid dipolar broadening in model cluster EPR (cf. Ref. *47*). We also assume that the cluster has not been enriched in ^{57}Fe and/or ^{33}S. Thus the only possible interactions, in addition to the Zeeman term of Eq. (16), are superhyperfine interactions with magnetic nuclei in the second and higher coordination sphere, i.e., ^{1}H, ^{13}C, and ^{14}N from the protein (and, possibly, ^{14}N from coordinating His in the Rieske cluster). In standard continuous wave EPR, these ligand splittings are usually not resolved, but rather contribute to the inhomogeneous line width. In magnetic field units this contribution should be independent of the frequency of the applied microwave. Experimentally, however, one usually finds that the EPR line width from biological $S = \frac{1}{2}$ systems has a major contribution that is linear in the microwave frequency. Figure 4 gives the example of the $[2Fe–2S]^{1+}$ cluster in spinach leaf ferredoxin (note: each point is from a different spectrometer). At the common X-band frequency the broadening is essentially dominated by a mechanism linear in the microwave frequency. This observation strongly suggests that the line width reflects a type of Zeeman interaction.

We want to analyze the EPR spectrum by the method of spectral synthesis. This means that we want to faithfully reproduce the experimental spectrum on a computer using a theoretically founded algorithm. There are two good but very different reasons why we want to achieve this goal. In the first place, this simulation technique is the only way in which we can separate in a quantitative manner the fine spectral details (the "tertiary magnetic structure" of the cluster reflecting the specific protein environment) from the more general fea-

tures common to all clusters of a given type. A second objective is the analysis of compound data, i.e., overlapping spectra from different centers in complex systems. A classical example of this latter problem is the determination of the number, type, and stoichiometry of paramagnets in respiratory chain complexes (cf. Refs. *126* and *127*).

The technique of simulating "powder" spectra (e.g., spectra from frozen solutions of metalloproteins) is well established (*128*). The powder pattern is generated by computing individual spectra for many different orientations and adding them all up. This is called integration over the unit sphere:

$$\chi'' = \int\int P(g)\, S(g, W)\, d\cos\Theta\, d\phi \tag{17}$$

$S(g, W)$ is a shape function, usually a Gaussian of width W, whose peak position follows from Eq. (16):

$$B_{\text{resonance}} = (h/\beta)\nu/g \tag{18}$$

in which

$$g = \sqrt{l_x^2 g_x^2 + l_y^2 g_y^2 + l_z^2 g_z^2} \tag{19}$$

The g_i values are the principal values of the g tensor. The l_i values are the direction cosines of the magnetic field vector with respect to the g-tensor axis system. They translate in polar angles as

$$\begin{aligned} l_x &= \sin\Theta\cos\phi \\ l_y &= \sin\Theta\sin\phi \\ l_z &= \cos\Theta \end{aligned} \tag{20}$$

$P(g)$ is the transition probability (*129*):

$$P(g) = g^{-1}\Sigma(g_i^2 - g^{-2} l_i^2 g_i^4) \tag{21}$$

This is all standard procedure. However, the line width, W, is experimentally found to be orientation dependent, i.e., a function of the direction cosines. Our problem is that we do not know what the analytical expression of this dependence is.

Two ad hoc solutions have been proposed (and subsequently applied in too many cases to be comprehensively reviewed here). The algorithm of Johnston and Hecht (*130*),

$$W = \sqrt{l_x^2 W_x^2 + l_y^2 W_y^2 + l_z^2 W_z^2} \tag{22}$$

is simply an analog of the g value, Eq. (19), suggestive of a distribution of the g values themselves. One could call this the simplest possible

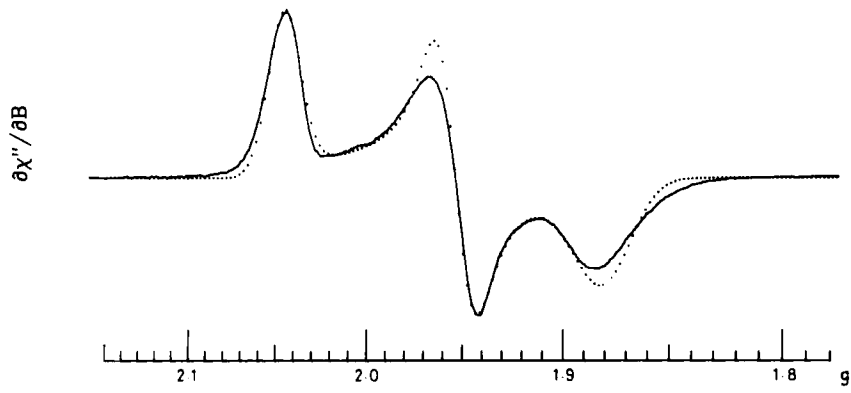

FIG. 5. The X-band spectrum of the reduced [2Fe–2S] cluster in spinach ferredoxin (solid trace) is computer simulated (dots) with a line width anisotropy according to Eq. (23) (*132*).

form of "g strain," a term that was proposed several years later in the group of Sands and his collaborators (*16, 108*).

A second proposal, due to Venable (*131*),

$$W = \sqrt{l_x^2 g_x^4 W_x^2 + l_y^2 g_y^4 W_y^2 + l_z^2 g_z^4 W_z^2}/g^2 \tag{23}$$

is an analog of the expression for the first-order central hyperfine splitting in orthorhombic symmetry:

$$A = \sqrt{l_x^2 g_x^4 A_x^2 + l_y^2 g_y^4 A_y^2 + l_z^2 g_z^4 A_z^2}/g^2 \tag{24}$$

Although Eq. (23) is probably the most frequently used expression in work on iron–sulfur proteins (cf. Ref. *127*), it cannot possibly be correct: there is no central (i.e., metal) hyperfine interaction in Fe–S clusters; ligand hyperfine interaction is negligible; the line width is not independent of the microwave frequency.

In practice, the two proposed solutions, Eqs. (22) and (23), give virtually indistinguishable results. This is a consequence of the fact that they both describe an effective line width tensor that is colinear with the g tensor. The appearance of the powder spectrum is dominated by the turning points of the g value, Eq. (19). What happens off-axis is to a large extent irrelevant to the overall spectral shape. Unfortunately, both solutions give poor results. A typical illustration is given in Fig. 5 (*132*). The word "typical" here indeed means exemplary for very many simple $S = \frac{1}{2}$ spectra. The low-field peak and the high-field trough in the experimental spectrum are skewed, and this is not reproduced in the fit. Similarly, the asymmetry of the derivative-shaped feature is not

simulated. These asymmetries are the easily recognizable trademark of g-strain broadening.

Over the past 25 years a dozen attempts have been made toward a more sophisticated approach of the line width problem in biological EPR. These studies were mainly concerned with hemoproteins (cf. references quoted in Ref. *126*); however, some of the more recent ones address the problem in relation to specific types of iron–sulfur proteins (*24, 133*). The central idea in all the proposed theories is to have a distributed effective g values by assuming a symmetric distribution in one or more quantities that directly define the effective g value itself. Thus, distributions have been proposed in crystal field splittings, spin–orbit interactions, ground state wave function coefficients, or coefficients in the spin Hamiltonian. All the proposed models approximately simulate the magnitudes of line width anisotropy; however, they *never* generate the skewings and asymmetries of real g strain.

We must, therefore, conclude that the cause of g strain and the cause of the g tensor are two entities of a completely different nature. Somewhere in between these entities is an angular transformation resulting in a noncollinearity of tensor quantities.

B. The g-Strain Equation and Its Implications

Fritz *et al.*, who first proposed the term "g strain," also suggested a model for its physical nature: microheterogeneity in protein conformation (*16*). Taking the strain in g strain literally, the present author later proposed to include a strain term in the spin Hamiltonian to describe effects of the matrix surrounding the protein (i.e., the frozen solvent) on the protein and the spin system within (*134*). The resulting equation for the angular-dependent line width (*132, 134*) for the first time allowed for a line width tensor to be noncollinear with the g tensor. Its implementation in a spectrum simulation program for the first time closely reproduced the asymmetries of g strain in powder spectra of a low-spin hemoprotein (*134*) and an iron–sulfur protein (*132*). The program was also original in calculating spectra in g space with subsequent transformation to field space. This idea was based on the notion, proposed by Strong (*135*), that the distribution function due to g strain is necessarily nonlinear on a magnetic field scale. However, the line width algorithm (*132, 134*) was not the result of a rigorous derivation, and in a later study it was shown to contain an error of normalization (*136*).

Combining the idea of a noncollinear line width tensor (*132, 134*) with the statistical concept of the g values as random variables (*97*),

two groups working on the problem of g strain joined forces and developed the statistical theory of g strain (*136*). This theory was derived from the single premise that the g tensor is a linear function of a three-dimensional random variable:

$$\mathbf{g} = \mathbf{g}_0 + \mathbf{R} \cdot \mathbf{p} \cdot \mathbf{R}^{\mathrm{T}} \tag{25}$$

Here, $\mathbf{p}$ is a tensor whose elements are random variables, $\mathbf{g}_0$ is a tensor whose elements do not fluctuate, and $\mathbf{R}$ is the three-dimensional rotation that transforms the $\mathbf{p}$ principal axis system to the $\mathbf{g}_0$ principal axis system. The resulting expression for the angular-dependent line width turned out to be a discouragingly complicated one, both in form and in its amenability to use in numerical analysis (*136*). It contains, e.g., a five-dimensional rotational transformation.

The problem was saved from intractability by an unexpected finding (*136*): when the three elements of the $\mathbf{p}$ tensor in Eq. (25) are statistically fully correlated (either positively or negatively), then the complicated five-dimensional expression reduces to a much simpler, three-dimensional expression; this turns out to be a normalized version of the successful (but not rigorously derived) expression in the early work (cf. Refs. *132* and *134*).

There is also a plausible physical interpretation of this result. When all the elements of the tensor describing g strain are fully correlated, then their ultimate cause must be a scalar. This scalar can be identified with a hydrostatic pressure exerted on the paramagnetic protein by its surroundings, the matrix of the (frozen) solution (*126*). Here is a simple picture to envisage the process: the outside of the protein is a globe. Inside is an iron–sulfur cluster, say a cubane, which is connected to the inner surface of the globe by means of a complicated network of strings (the protein structure). A hydrostatic pressure, or uniform stress on the globe is transduced onto the cubane as a strain with directional properties (the $\mathbf{p}$ tensor) *un*related to the structure of the cube (the $\mathbf{g}_0$ tensor).

The unrestricted form of the statistical theory of g strain has been tested on high-quality multifrequency data from $[2Fe–2S]^{1+}$ ferredoxins, resulting in (1) very good fits, and (2) proof of full correlation between the $\mathbf{p}$-tensor elements (*25*). Figure 6 gives an example of such a fit. In spite of some initial difficulties (*137*) and concern (*138*), it now appears that fully correlated g strain is also an adequate model for inhomogeneously broadened EPR from $[4Fe–4S]^{3+}$ in HiPIPs (*125*) as well as from $[4Fe–4S]^{1+}$ in ferredoxins (W. R. Dunham, personal communication, 1990) and in complex enzymes (*139*). It is also operative

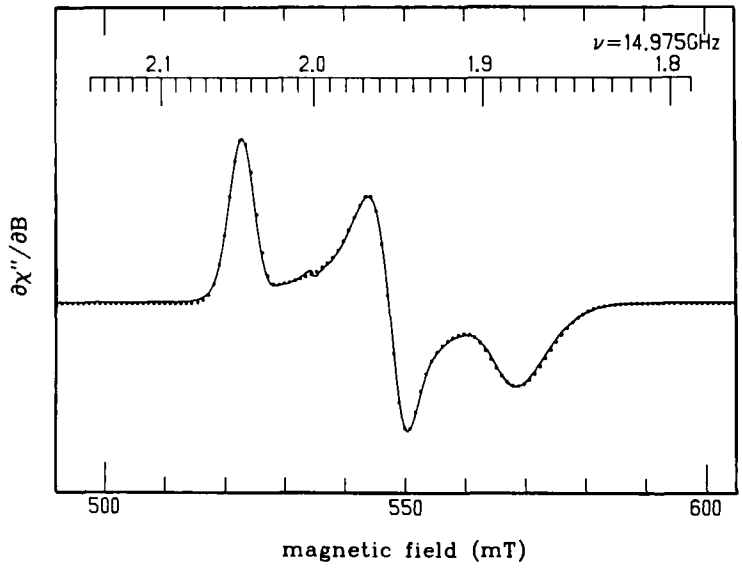

FIG. 6. The P-band spectrum of the reduced [2Fe–2S] cluster in *Synechococcus lividus* ferredoxin (solid trace) is computer simulated (dots) with a line width anisotropy according to Eq. (26), the g-strain equation (*25, 139*).

in biological $[3Fe–4S]^{1+}$ clusters (*107*) and in $[6Fe–6S]^{3+}$ prismane cores in model compounds (*47*).

The g-strain equation is

$$W = |l_x^2 g_x \Delta_{xx} + l_y^2 g_y \Delta_{yy} + l_z^2 g_z \Delta_{zz} + 2l_x l_y \sqrt{g_x g_y}\,\Delta_{xy} + 2l_x l_z \sqrt{g_x g_z}\,\Delta_{xz} + 2l_y l_z \sqrt{g_y g_z}\,\Delta_{yz}|/g \tag{26}$$

Its derivation can be found in Ref. *136* and is not repeated here. Note that in the original work this equation was given in a compact matrix notation [Eq. (34) in Ref. *136*; see also Ref. *126*). Equation (26) accurately describes the angular-dependent line width in the above-mentioned iron–sulfur systems. The line width, W, is interpreted as the variance of g in Eq. (25) when the principal g values are functions of fully correlated random variables. Equation (26) follows from a general statistical model that does not assume anything about the physical nature of g strain, other than that the full correlation implies the ultimate cause of g strain to be a scalar quantity. In other words, Eq. (26) provides a practical means to effectively describe line broadening in the EPR of iron–sulfur $S = \frac{1}{2}$ systems while leaving ample room for future theorization on the molecular mechanisms involved.

The Δ values in Eq. (26) are the six independent elements of a 3×3 real, symmetric matrix. This matrix describes the **p** tensor of Eq. (25) in the axis system that diagonalizes the **g** tensor. The Δ values also have a practical interpretation as *g*-strain parameters. The absolute values of the diagonal elements Δ_{ii} are to a good approximation equal to the apparent line width on a *g*-value scale of the three features of the powder spectrum. Their approximate value can be read from the experimental spectrum. The off-diagonal elements, Δ_{ij}, are responsible for the typical asymmetries in *g*-strain broadened spectra. Their value can not be read from the spectrum, therefore analysis of *g*-strained spectra always requires computer simulation. Because the Δ values reflect a distribution in effective *g* values, these simulations have to be made in *g* space, and the resulting spectrum has to be subsequently transformed to *B* space for comparison with experimental data (*139*).

The numerical values of Δ can be positive or negative. This has the implication that the line width from *g* strain can be zero for some molecules that do not have their **g** tensor aligned with the external magnetic field (i.e., for some intermediate orientations). As an important practical consequence the computation time required for simulations based on Eq. (26) increases by some two orders of magnitude compared to simulations based on the ad hoc algorithms of Eq. (22) or (23). A number of tricks on how to handle this problem numerically are detailed elsewhere (*139*).

It appears to be generally accepted nowadays that *g* strain is an important determinant for the EPR spectral shape of iron–sulfur proteins. Frequently, however, the concept of *g* strain is only referred to parenthetically, and quantitative analysis is not attempted. Reluctance to apply Eq. (26) may be related to its complicated mathematical background (*136*) and to the nontrivial character of its numerical analysis (*139*). This reviewer hopes for increased efforts in the future, which he advocates as follows. EPR spectral analysis of iron–sulfur proteins using the *g*-strain concept provides more accurate *g* values (*93*); it gives better deconvolutions of complex spectra from multicenter proteins and, therefore, more reliable stoichiometry numbers (*139*); it should give information—by systematic comparison—on the internal flexibility/rigidity of proteins (*25*). A direct link has also been suggested between *g* strain and spin lattice relaxation; a rudimentary theory based on this idea had some success in describing continuous wave saturation of the $[2Fe–2S]^{1+}$ EPR from spinach ferredoxin (*132*). This suggestion has not incited any response in the decade following its proposal.

IV. High-Spin Kramers' Systems

A. The Weak-Field Regime

As with g strain, this is another field of biological EPR whose development is presently dominated by examples from iron–sulfur EPR. The biological superspins ($S > \frac{5}{2}$) are unknown outside the Fe–S field. We have already pointed to their association with putative iron–sulfur superclusters. Remarkably, the $S = \frac{5}{2}$ system is a relative rarity for iron–sulfur clusters in contrast to its ubiquity in iron–protein EPR in general. On the other hand, the $S = \frac{3}{2}$ system appears to be limited to the domain of iron–sulfur and mixed-metal iron–sulfur clusters, except for the cases of high-spin ferrous NO (*140*) and high-spin cobaltous proteins (*141*).

Half-integer high-spin systems in biology have been analyzed with the spin Hamiltonian:

$$H = \mathbf{S} \cdot \mathbf{D}' \cdot \mathbf{S} + \beta \mathbf{B} \cdot \mathbf{g} \cdot \mathbf{S} \tag{27}$$

For $S > \frac{3}{2}$, higher order terms in S are allowed theoretically (*142*), but this theme has only rarely been touched in biological EPR (*143, 144*). There is a practical difficulty in discerning between the effects of higher order terms and the second-order term, $\mathbf{S} \cdot \mathbf{D}' \cdot \mathbf{S}$, in half-integer spin systems (see, e.g., Ref. *145*). The subject has thus far been completely ignored in iron–sulfur EPR. We have nothing to add here (but we will have, below, when discussing non-Kramers' systems).

A characteristic aspect of high-spin metalloprotein EPR, including all high-spin iron–sulfur EPR, is the general validity at X-band frequencies of the inequality

$$\mathbf{S} \cdot \mathbf{D}' \cdot \mathbf{S} \gg \beta \mathbf{B} \cdot \mathbf{g} \cdot \mathbf{S} \tag{28}$$

In this "weak-field limit," the $S = n/2$ multiplet forms $(n + 1)/2$ Kramers' doublets, each of which is separated from the others by energies significantly larger than the $\approx 0.3\text{-cm}^{-1}$ microwave quantum. On the other hand, all the doublets within the ground multiplet are at sufficiently low energies to be significantly populated in the temperature range practical for iron–sulfur EPR, typically from 4 to 100 K. In this situation, each doublet of the $S = n/2$ system is expected to give rise to its own resonance, which can be described in terms of an effective $S = \frac{1}{2}$ spectrum with three effective g values. For example, an $S = \frac{9}{2}$ system will have a superposition of five $S_{\text{eff}} = \frac{1}{2}$ spectra with a total of 15 effective g values. However, not all of these g_{eff} values are observables, as will become obvious below. A practical way to analyze these

types of spectra is in terms of a single quantity, the rhombicity parameter, making use of a graphical representation of tabular values, for which I have proposed the name "rhombograms."

B. Calculation of Effective g Values

Since the zero-field interaction tensor, $\mathbf{D}'$, is traceless, one usually rewrites the term $\mathbf{S} \cdot \mathbf{D}' \cdot \mathbf{S}$ in the two-parameter form:

$$H_{ZF} = D[S_z^2 - S(S + 1)/3] + E(S_x^2 - S_y^2) \tag{29}$$

and this allows us to define "rhombicity" as a single parameter, E/D, whose value is limited theoretically as (*146, 147*):

$$0 \leq |E/D| \leq \tfrac{1}{3} \tag{30}$$

Note that some authors prefer to define a rhombicity parameter, η, in a slightly different manner, namely, $\eta \equiv 3E/D$, as this limits the magnitude of rhombicity between zero and unity.

We assume the $\mathbf{D}'$ and $\mathbf{g}$ tensor to be collinear, and we write out the Zeeman interaction in a shorthand notation as

$$H_{Zeeman} = G_x S_x + G_y S_y + G_z S_z \tag{31}$$

with

$$G_i = g_i l_i \beta B S_i \qquad (i = x, y, z) \tag{32}$$

The direction cosines, l_i, were defined in Eq. (20). With the spin functions for the $S = n/2$ system written as

$$|m_s\rangle = |n/2\rangle; |(n - 1)/2\rangle; \ldots; |-n/2\rangle \tag{33}$$

and recalling that

$$\begin{aligned} S_z|m_s\rangle &= m_s|m_s\rangle \\ S_+|m_s\rangle &= \sqrt{S(S + 1) - m_s(m_s + 1)}|m_s + 1\rangle \\ S_-|m_s + 1\rangle &= \sqrt{S(S + 1) - m_s(m_s + 1)}|m_s\rangle \\ S_x &= (\tfrac{1}{2})(S_+ + S_-) \\ S_y &= (\tfrac{1}{2}i)(S_+ - S_-) \end{aligned} \tag{34}$$

we can now construct the energy matrix by calculating all the matrix elements $\langle m_s|H|m_s'\rangle$.

For example, for $S = \frac{3}{2}$ we have

$$|m_s\rangle = |\tfrac{3}{2}\rangle; |\tfrac{1}{2}\rangle; |-\tfrac{1}{2}\rangle; |-\tfrac{3}{2}\rangle \tag{35}$$

and the energy matrix is

	$\lvert+\frac{3}{2}\rangle$	$\lvert-\frac{3}{2}\rangle$	$\lvert+\frac{1}{2}\rangle$	$\lvert-\frac{1}{2}\rangle$
$\langle+\frac{3}{2}\rvert$	$D + 3G_z/2$	0	$\sqrt{3}\,(G_x - iG_y)/2$	$E\sqrt{3}$
$\langle-\frac{3}{2}\rvert$	0	$D - 3G_z/2$	$E\sqrt{3}$	$\sqrt{3}\,(G_x + iG_y)/2$
$\langle+\frac{1}{2}\rvert$	$\sqrt{3}\,(G_x + iG_y)/2$	$E\sqrt{3}$	$-D + G_z/2$	$G_x - iG_y$
$\langle-\frac{1}{2}\rvert$	$E\sqrt{3}$	$\sqrt{3}\,(G_x - iG_y)/2$	$G_x + iG_y$	$-D - G_z/2$

(36)

The equivalent matrices for $S = \frac{5}{2}; \frac{7}{2}; \frac{9}{2}$ and their application to iron–sulfur protein EPR can be found in Refs. *49* and *54*. There are two ways to use these matrices for the interpretation of high-spin EPR data: the exact solution and the weak-field approximation. These approaches are similar in conception; however, they differ drastically in their practical applicability.

The exact solution is obtained as follows. Numerical diagonalization of the energy matrix gives the relative energies of the $n + 1$ levels within the $S = n/2$ multiplet. To find the effective g values of the EPR spectrum, we carry out the diagonalization along the principal axes (D' and g are collinear), i.e., for the three possibilities,

$$(l_x, l_y, l_z) = (1, 0, 0); \quad (0, 1, 0); \quad (0, 0, 1) \tag{37}$$

We choose values for the fitting parameters D, E, g_x, g_y, and g_z and subsequently do the diagonalization along each axis for many different values of the external magnetic field, B, in order to find all those B values for which two of the $n + 1$ energy levels differ by an amount, ΔE, equal to the energy of the applied microwave quantum. We then get the effective g values from the resonance condition:

$$g_{\text{effective}} = \Delta E/(\beta B) \tag{38}$$

The amounts of CPU time required by this approach may well be prohibitive in many practical applications.

In the weak-field limit [cf. Eq. (28)] the Zeeman term is only a small perturbation to the zero-field interaction. A significant consequence of this is that the effective g values are frequency independent. In practice, substituting any "large" value for D and any "small" value for B in the energy matrix results in the same set of effective g values. Typical

dummy values can be anywhere within the range $10 < D < 100$ cm^{-1}, and $0.01 < B < 1$ T. The complexity of the problem is now considerably reduced, because the matrix diagonalization has to be done for a single B value only, and also because the g_{eff} values no longer depend on the values of D and E, but only on their ratio, E/D.

A further simplification ensues from the realization that the g_{eff} values shift much more significantly by changes in the value of E/D than by deviations in the *real* g values from the free-electron value. In other words, we can, as a reasonable starting point, assume that the real g values are

$$g_x = g_y = g_z = 2.00 \tag{39}$$

This should be a good assumption for the $3d^5$ system with quenched orbital angular momentum, e.g., Fe(III) in rubredoxin. It should also be a rather good assumption for iron–sulfur systems, especially for the most oxidized ones. There are few reports on attempts to document deviations from Eq. (39) in high-spin EPR from iron–sulfur proteins. A real $g_z \approx 2.04$ was deduced from the $S = \frac{3}{2}$ EPR from the iron–molybdenum cofactor in dithionite-reduced nitrogenase (*148, 149*). For the equivalent spectrum from the vanadium-containing nitrogenase, $g \approx 2.06$ has been reported (*150*). In general, it would appear that the deviations in high-spin iron–sulfur EPR are maximally of the order of a few digits in the second decimal place of the real g values, and this is probably comparable to the uncertainty in the effective g values due to our limited understanding of the details of the line shapes in these spectra.

With the three elements of the real g tensor fixed at 2.00, and the value of the axial zero-field parameter, D, irrelevant, we find that any half-integer high-spin system has an EPR spectrum that is a function of a single parameter only, i.e., the rhombicity E/D. This allows us to analyze these spectra by means of simple, two-dimensional graphs of effective g values versus rhombicity.

C. The Reading of Rhombograms

Rhombograms for the cases $S = \frac{3}{2}, \frac{5}{2}, \frac{7}{2}$, and $\frac{9}{2}$ are given in Fig. 7 (A–D) (*54, 69, 147, 151*). All possible g values for the subspectrum from a particular Kramers' doublet are represented by the three curves in the individual panels. Spectral analysis means now simply placing a ruler parallel to the vertical axes of Fig. 7 and moving it along the horizontal axes to a rhombicity that produces all the experimentally observed effective g values. Thus graphically determined approximate values

can be checked with more accurate computer calculations. These calculations also allow for trials with real g values deviating from 2.00. A simple, efficient program running on personal computers is available from the author (*152*). In practice, three types of problems can occur: (1) not all the theoretically predicted effective g values are observed, (2) the system has more than one discrete rhombicity, and (3) the system is a mixture of different spins (the latter two problems will be addressed separately below).

It should be evident from a quick glance at Fig. 7 that in many cases some of the effective g values are simply too low to be detected. The maximum value for the electromagnet of an X-band EPR spectrometer is typically of the order of 1 T. This excludes detection of all $g < 0.6$. The problem can not be solved simply by the application of higher magnetic fields, because this would take us out of the weak-field regime, leading to a breakdown of Eq. (28) and, therefore, of the validity of the

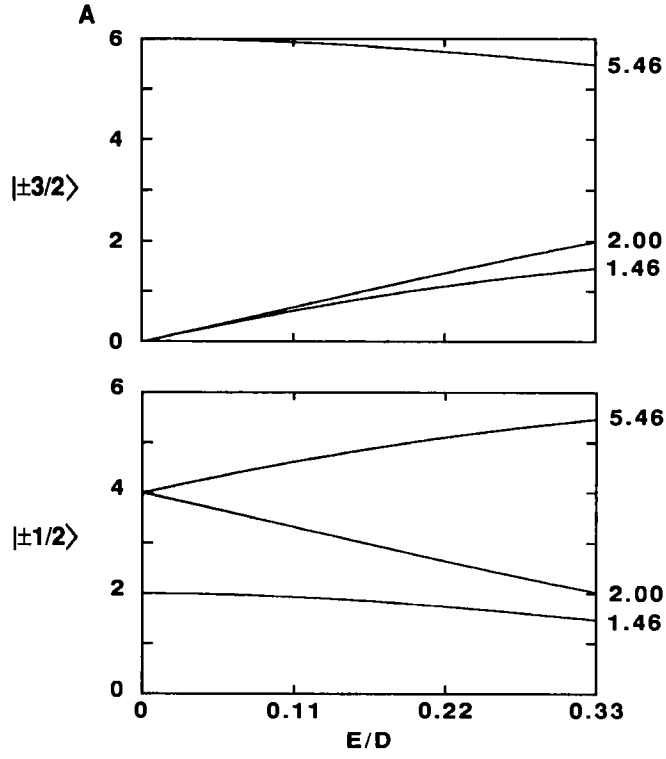

FIG. 7. Rhombograms: (A) $S = \frac{3}{2}$; (B) $S = \frac{5}{2}$; (C) $S = \frac{7}{2}$; (D) $S = \frac{9}{2}$.

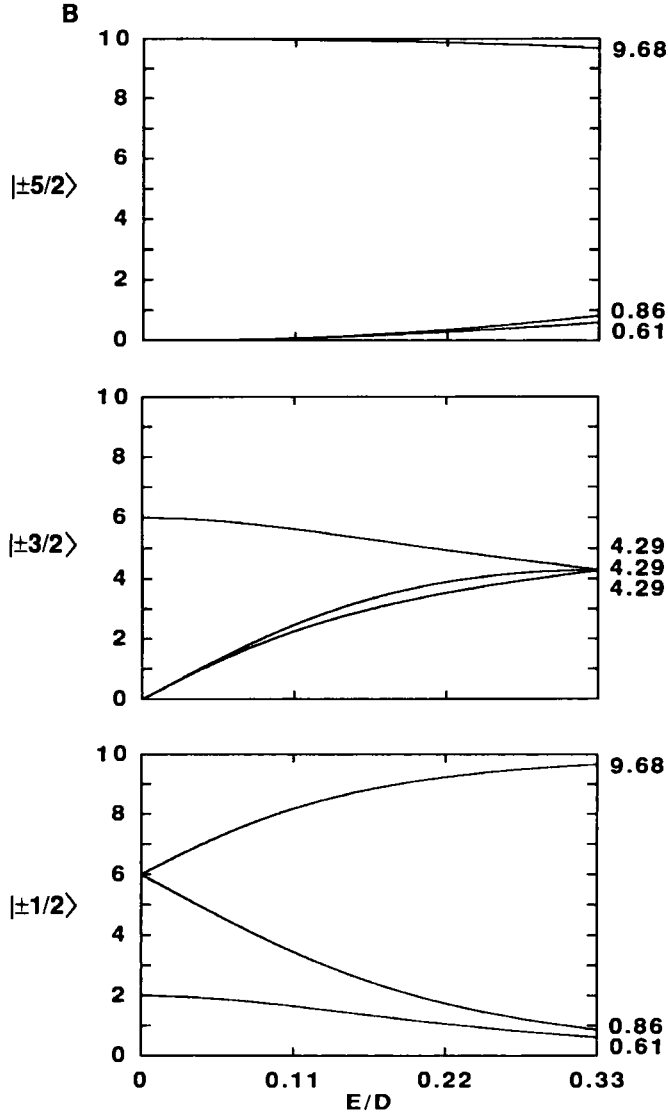

FIG. 7 (*continued*).

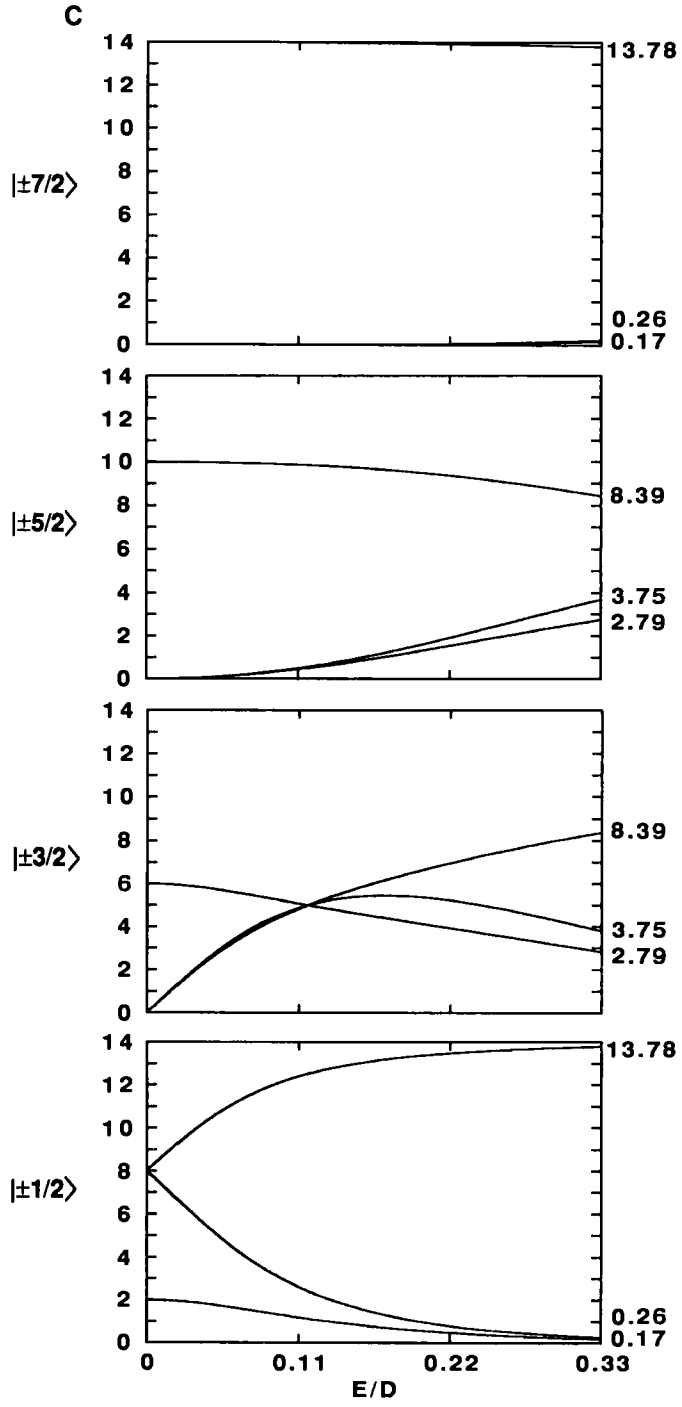

FIG. 7 (*continued*).

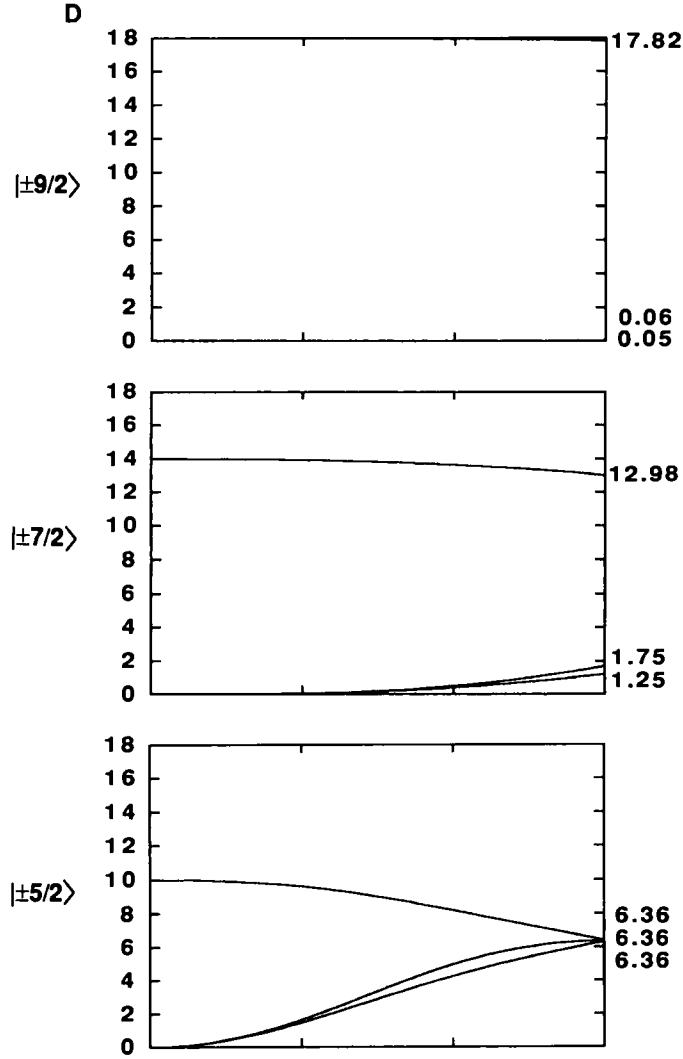

FIG. 7 (*continued*).

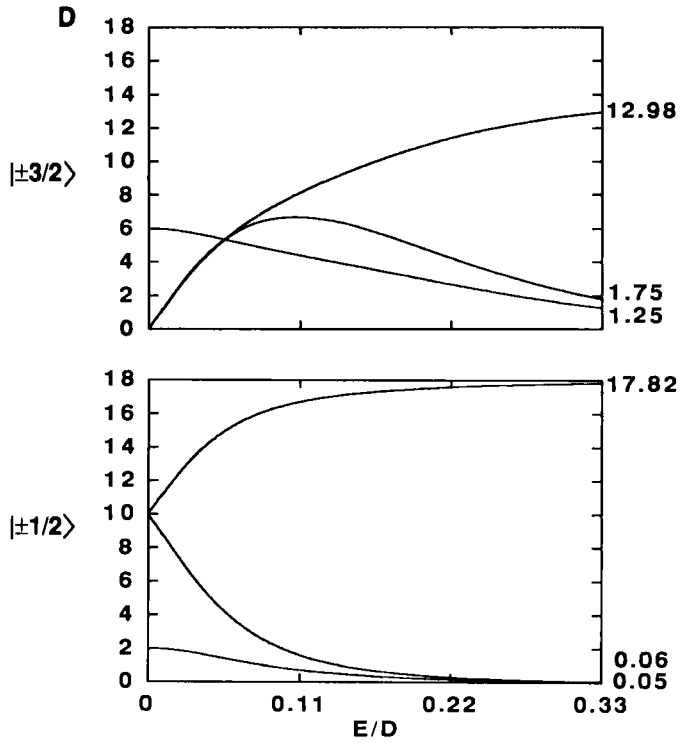

FIG. 7 (*continued*).

diagrams in Fig. 7. A closely related problem is that of the low intensity of highly anisotropic spectra. In the axial case (i.e., $E = 0$), no spectrum other than that from the $|\pm\frac{1}{2}\rangle$ doublet is observable. All the other doublets have two g values outside the magnetic field range, $g_x = g_y = 0$. The third g value always corresponds to a practical field value; however, it is also not observed because the transition probability is zero [cf. Eq. (21)]. Reworded, an infinitely wide spectrum has infinitely low intensity, or the smaller the g anisotropy the higher the spectral intensity will be. This notion leads to three rules of thumb relating to the intensity of subspectra from half-integer spins:

Rule 1: the likelihood of observing a transition within the higher doublets increases with increasing rhombicity, E/D.

Rule 2: this likelihood decreases with increasing system spin, S.

Rule 3: the likelihood also decreases with increasing projected spin, m_s.

Consider some examples to illustrate these rules. The molybdenum–iron cofactor in nitrogenase is an $S = \frac{3}{2}$ system with a relatively low rhombicity value, $E/D = 0.055$ (*148*). The spectrum from the $|\pm\frac{3}{2}\rangle$ doublet is extremely weak and is difficult to detect (*149*). When the cofactor is isolated from the protein, the rhombicity increases ($E/D = 0.11$) and the excited state EPR becomes readily observable (*153*). In the vanadium-containing nitrogenase the rhombicity has further increased to $E/D = 0.26$, and now the two subspectra have comparable intensity (*150*). The $S = \frac{5}{2}$ is poorly represented in the iron–sulfur proteins, therefore, we look at other iron proteins. Ferric high-spin hemoproteins are $S = \frac{5}{2}$ systems of low rhombicity. No EPR other than from the $|\pm\frac{1}{2}\rangle$ ground doublet has ever been observed. Highly rhombic $S = \frac{5}{2}$ systems are found in mononuclear ferric centers. In some cases EPR from all three doublets is observable (*69, 154*). Data on Fe–S (or Fe–Se) $S = \frac{7}{2}$ and $S = \frac{9}{2}$ systems are presently limited to two (*49, 84*) and four (*51, 54, 56, 57*) cases, respectively. EPR from the highest doublet has not been observed for any of these systems. EPR from the second highest doublet is, at best, only indicated in one or two cases (*49, 57*).

A fourth rule of thumb applies to the (lower) intermediate doublets. Again, by inspection of Fig. 7 it is obvious that systems with $S \geq \frac{5}{2}$ have at least one doublet with three coinciding g values for a particular value of the rhombicity parameter. An actual rhombicity close to this value will lead to a near-isotropic subspectrum of relatively high intensity. It is helpful to realize that the rhombograms of Fig. 7 possess a graphical symmetry in the sense that extending the lowest panel along the horizontal axis to the range $\frac{1}{3} \leq E/D \leq 1$ results in the (stretched) mirror image of the upper panel (cf. Ref. *147*). The same operation on the next to the lowest panel gives the mirror image of the second highest panel. For those systems that have an odd number of Kramers' doublets (i.e., $S = \frac{5}{2}, \frac{9}{2}, \frac{13}{2}$, etc.), extension of the middle panel should produce its own mirror image. These systems all have an isotropic spectrum at maximal rhombicity, i.e., $E/D = \frac{1}{3}$. For $S = \frac{5}{2}$ this gives rise to the well-known $g = 4.3$ line, whose isotropy allows for the detection of small quantities of adventitiously bound ferric ion in biological preparations. The equivalent of this for $S = \frac{9}{2}$ systems is an isotropic line at $g = 6.4$. The first putative detection of an $S = \frac{9}{2}$ system with $E/D \approx \frac{1}{3}$ has recently been made (*57*).

In addition, systems with $S \geq \frac{7}{2}$ have another doublet with coinciding g values for intermediate values of E/D. For a real g value of 2.00 we find for the next to the lowest doublet of an $S = \frac{7}{2}$ system an isotropic spectrum with $g = 5.00$ ($E/D = 0.117$). And for an $S = \frac{9}{2}$ system there

is an isotropic spectrum with $g = 5.34$ ($E/D = 0.055$). Actual systems with a rhombicity close to any of the quoted values are likely to have an easily detectable, near-isotropic subspectrum. Examples are found in the $S = \frac{7}{2}$, $g \approx 5.2$ EPR from selenium-substituted ferredoxin (*83, 84*) and in the recently reported $S = \frac{9}{2}$, $g \approx 5.7$ EPR from the putative prismane protein (*52, 55, 59*) and from a carbon monoxide dehydrogenase (*56*). We summarize the previous statements:

Rule 4: near-isotropic, therefore easily detectable, subspectra occur for the middle doublet in maximally rhombic $S = \frac{5}{2}$ or $\frac{9}{2}$ systems and for the $|\pm\frac{3}{2}\rangle$ doublet from $S = \frac{7}{2}$ or $\frac{9}{2}$ systems of intermediate rhombicity.

Finally, we must consider the angular dependency of the line width as well as the dependency on m_s. Since the theoretical description of line width in high-spin systems is undeveloped, we have to rely on a few practical observations plus some very rudimentary theory. From early work on high-spin ferric heme in myoglobin ($S = \frac{5}{2}$, $|\pm\frac{1}{2}\rangle$ EPR, $E/D \approx 0$) it was concluded that the effective g values were distributed as a consequence of the combined effects of g strain in the real g values and a distribution in the parameter E, the latter effect being rather strongly angular dependent (*134*). Similarly, we have found for other, more rhombic systems, such as for the mononuclear high-spin ferric site in *Escherichia coli* superoxide dismutase with $E/D = 0.24$ (*155*), that the inhomogeneous line width results from the combined effects of g strain and a distributed rhombicity. Since the real **g** tensor in the present approach is taken to be (near) isotropic, the line width from g strain is isotropic in magnetic field units. On the other hand, a distributed E value results in line widths that increase very rapidly with increasing magnetic field, i.e., with decreasing effective g value. Considering attempts at further theorization on the subject to be presently premature, I simply summarize a limited set of phenomenological observations:

Rule 5: within a subspectrum the line width in field units usually increases (therefore, the intensity decreases) rather rapidly with decreasing effective g value; lines of different subspectra with similar effective g values have line widths of the same order of magnitude.

When taking all the five rules of thumb together the following picture emerges. Near-axial systems will exhibit the $|\pm\frac{1}{2}\rangle$ subspectrum only. With increasing rhombicity the $|\pm\frac{1}{2}\rangle$ subspectrum becomes more difficult to detect, and subspectra from higher doublets become significant. Sometimes the mathematical coincidence of effective g values causes

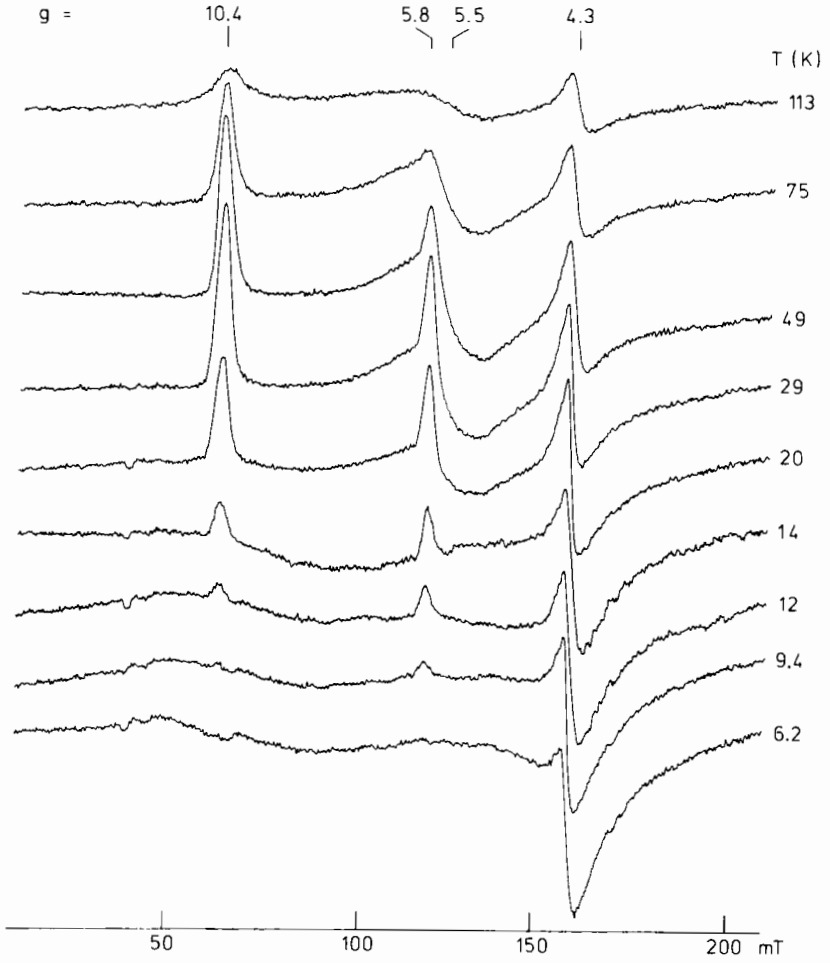

FIG. 8. Temperature dependence of the $S = \frac{1}{2}$ X-band EPR of the P-cluster in thionine-oxidized nitrogenase Mo–Fe protein from *Azotobacter vinelandii* (*49*).

one of the intermediate subspectra to become dominant. With increasing system spin it is increasingly difficult to detect EPR from the highest doublets.

D. PRACTICAL ASPECTS OF IRON–SULFUR HIGH-SPIN EPR

Figure 8 shows the temperature dependence of part of the X-band spectrum from thionine-oxidized Mo–Fe protein of nitrogenase (*49*).

The spectrum is from an $S = \frac{7}{2}$ superspin assigned to the P-cluster, a putative iron–sulfur supercluster (*49, 63*) of otherwise undefined structure. Figure 8 is a convenient example to illustrate the intensity rules derived in the previous section, and to discuss additional practical aspects.

The rhombicity of the $S = \frac{7}{2}$ system is $E/D = 0.043$. This value is consistent with a $|\pm\frac{1}{2}\rangle$ subspectrum with $g = 10.4$, 5.4, and 1.8 (cf. Fig. 7C). We do not observe this subspectrum below $T \approx 10$ K but only at intermediate temperatures (Fig. 8). The $S = \frac{7}{2}$ multiplet is upside down as a result of the D value being negative. This is probably the major reason why the—in principle easily detectable—spectrum of Fig. 8 has escaped detection for a number of years (*156–159*). In recent times it has become increasingly evident that inverted multiplets are the rule rather than the exception in iron–sulfur $S = \frac{3}{2}$ (*150, 151, 160, 161*), $S = \frac{7}{2}$ (*49, 84*), and $S = \frac{9}{2}$ (*54–56*) systems. This had added importance to extended temperature variation in EPR, thus making the experiment more involved.

Possibly related to the inversion of the spin multiplet is the repeated observation that the EPR is not microwave saturable. All traces in Fig. 8 were recorded with 200 mW microwave power, typically the output of a leveled X-band klystron. Again, this nonsaturability appears to be the rule for high-spin, especially superspin Fe–S, systems. This not only means that current spectrometer performance is suboptimal with respect to the detection of these systems, but it also implies that superspins will probably not readily be studied by pulsed techniques and by double-resonance techniques.

In addition to the $|\pm\frac{1}{2}\rangle$ subspectrum, only the $|\pm\frac{3}{2}\rangle$ subspectrum is positively identified at $g_{\text{eff}} = 5.8$, consistent with out intensity Rules 1–3. The Rule 4-predicted mathematical coincidence of effective g values, resulting in near-isotropic subspectra, is not observed in this particular $S = \frac{7}{2}$ system. However, the isotropic line at $g = 4.3$ from a very small amount of adventitious iron ($S = \frac{5}{2}$) is a case in point. $S = \frac{9}{2}$ examples of this phenomenon may be found in the recently detected EPR spectra from different iron–sulfur proteins (*55, 57, 59*).

The Rule 5-predicted line width increase with decreasing effective g values is observed for the $g = 10.4$ and 5.5 features from the $|\pm\frac{1}{2}\rangle$ subspectrum.

We have indicated that the broadening described by Rule 5 is related to a distributed rhombicity. This smoothly varying, statistical distribution should be discriminated from a *discrete* distribution of rhombicities reflecting a limited number of discernible conformers. Only the latter results in resolved spectra from different components. For example, it

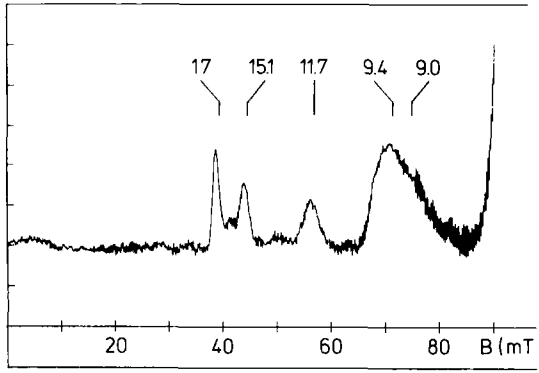

FIG. 9. Multiple rhombicities in the $S = \frac{9}{2}$ X-band EPR of the dissimilatory sulfite reductase from *Desulfovibrio vulgaris* strain Hildenborough (*54*).

is not at all uncommon to observe up to four different $|\pm\frac{1}{2}\rangle$ subspectra from $S = \frac{5}{2}$ hemoproteins and sirohemoproteins (cf. Refs. *54, 162,* and references quoted therein). The limited data presently available on $S = \frac{9}{2}$ systems in iron–sulfur proteins indicate that here discrete distributions in rhombicity are also a common phenomenon. An example is given in Fig. 9. The EPR from *D. vulgaris* sulfite reductase exhibits (at least) three sharp peaks at very high effective g values of 17, 15.1, and 11.7, and these have all been ascribed to the $|\pm\frac{1}{2}\rangle$ subspectrum from an $S = \frac{9}{2}$ system with discretely different rhombicities (*54*). Similar effects have been observed in the $S = \frac{9}{2}$ EPR form the putative prismane protein (*59*). These discrete distributions both in hemoproteins and in iron–sulfur proteins have thus far not been explained in (bio)chemical terms; they do present an additional complication in the spectroscopic analysis.

The spectrum of Fig. 9 also illustrates another practical rule for superspin EPR. From the rhombograms in Fig. 7 it can be seen that, in the weak-field limit, there is a maximum to g_{eff} for each particular system spin, namely, $g = 6$ ($S = \frac{3}{2}$), $g = 10$ ($S = \frac{5}{2}$), $g = 14$ ($S = \frac{7}{2}$), and $g = 18$ ($S = \frac{9}{2}$). This can be summarized in the simple rule:

$$g_{\max} \leq S \tag{40}$$

The observation of, e.g., $g = 17$ in spectrum of Fig. 9 identifies the system spin $S \geq \frac{9}{2}$.

The construction of the rhombograms, and every rule deduced from them, is based on the weak-field assumption. At higher magnetic field values, i.e., at lower effective g values, the assumption will increasingly

lose its validity. In attempts to evaluate this problem, rhombogram-predicted g values were compared to g values obtained from exact calculations for $S = \frac{7}{2}$ (*49*) and $S = \frac{9}{2}$ (*54*). Even for relatively small values of the zero-field splitting D (twice the X-band microwave quantum), the differences between the two methods became significant only for those lower effective g values that thus far have escaped detection. However, this is not necessarily true for data taken at higher microwave frequencies, as was shown by Aasa for the $S = \frac{5}{2}$ ferric transferrin (*163*).

At the end of our discussion of high-spin Kramers' systems we briefly consider an important but virtually unexplored theme (see Ref. *164* for a single exception): the validity of spin quantification procedures for high-spin systems. The quantification of $S = \frac{1}{2}$ spectra against that of an $S = \frac{1}{2}$ concentration standard is a well-established procedure (*128*). It is generally assumed—although nowhere explicitly stated in the vast literature on biological EPR—that this procedure also fully holds for Kramers' high-spin subspectra, provided correction is made for partial population according to Boltzmann statistics. However, no formal mathematical proof of this thesis has been given. There is ad hoc support in the practical finding that quantification of $|\pm\frac{1}{2}\rangle$ subspectra from high-spin systems usually gives a number that is an approximate multiple of the protein concentration. To what extend this "approximate" is a consequence of nonrigorous theory remains to be established. This caveat is emphasized for quantification on other than $|\pm\frac{1}{2}\rangle$ subspectra and on non-weak-field spectra.

V. Non-Kramers' Systems

A. Principles of Dual-Mode EPR in $S = 2$ Systems

We have seen that application of the spin Hamiltonian of Eq. (27) to half-integer spin systems ($S = n/2$) in the weak-field limit results in a grouping of levels within the spin multiplet into $(2n + 1)/2$ doublets. The same Hamiltonian applied to integer spin, or non-Kramers' systems ($S = n$), results in a grouping into n doublets and one singlet (see Fig. 10, left panel). Note, that these doublets are similar to the higher doublets of half-integer systems in that their associated subspectra in axial symmetry have two effective g values equal to zero. However, the two systems are *very* different with respect to the nature of the transition: Kramers' systems are subject to $|\Delta m| = 1$ transitions; non-Kramers' systems have $|\Delta m| = 0$ transitions. In quantum mechanical lan-

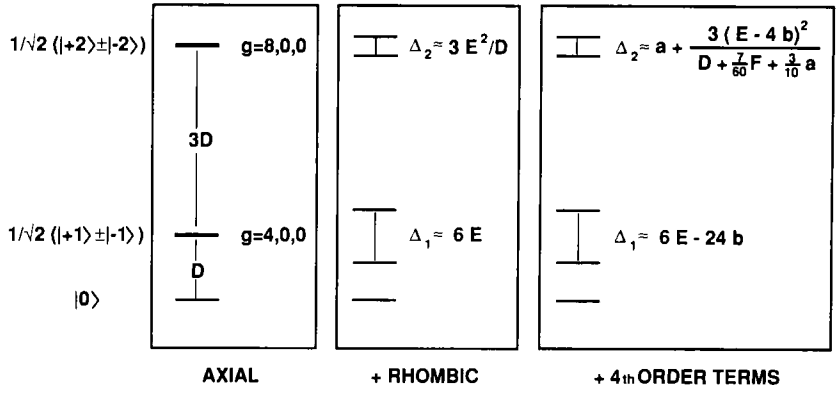

FIG. 10. Level scheme for the $S = 2$ multiplet under different zero-field spin Hamiltonians.

guage the two levels of a non-Kramers' doublet are not interconvertible by the time-reversal operator (*2*). An important consequence of this statement is that the two levels are not necessarily degenerate in a zero magnetic field. In fact, a finite rhombicity ($E \neq 0$) is sufficient to split the non-Kramers' doublet (Fig. 10). Kramers' doublets can never be split in zero field.

In axial symmetry ($E = 0$) the lowest three levels of Fig. 10 are admixed by the Zeeman interaction; therefore, a $|\Delta m| = 1$ transition within the first doublet is weakly allowed for all orientations except when the magnetic field is along the z axis. This transition is equivalent to the "half-field" transition with $g_{\text{eff}} \approx 4$ observed in many triplet ($S = 1$) systems. However, in the weak field limit this admixture is negligible, and no such subspectrum has ever been positively identified yet for iron–sulfur systems with $S \geq 2$. An additional complication here is that a finite rhombicity splits the doublet by an amount $\Delta_1 \approx 6E$, and this splitting can easily be greater than the energy of practically employed microwave quanta (*162*).

Rhombicity induces a much smaller splitting in the second doublet, $\Delta_2 \approx 3E^2/D$ for $S = 2$. It also mixes the levels of the doublet through coupling with the $|0\rangle$ singlet, and this creates the possibility to observe $|\Delta m| = 0$ transitions within the doublet (*2*). This requires a special experimental setup called parallel-mode EPR, in which the magnetic component of the microwave, B_1, is put parallel to the static magnetic field, B. In standard EPR spectrometers detecting $|\Delta m| = 1$ transitions, the common geometry is to have the vectors B and B_1 perpendicular. A

bimodal cavity is a resonator that can operate in each of the two modes, which are then typically separated in frequency by some 50 MHz (*144, 162*).

The approximate resonance condition for such non-Kramers' intradoublets transitions was formulated 40 years ago by Bleaney and Scovil (*165*) as

$$h\nu = \sqrt{(g_{\text{eff}}\beta B)^2 + \Delta^2} \tag{41}$$

Another simple and useful approximate rule (*166*) holds for the transition probability, or the intensity of the parallel-mode spectrum $I_{\parallel}$, at a given microwave frequency:

$$I_{\parallel} \propto \Delta^2 \tag{42}$$

The transition is also observable in a regular spectrometer except for those molecules that have their z axis exactly parallel to the static field B, i.e., $\Theta = 0$. In the neighborhood of the z axis we have (*167*)

$$I_{\perp}/I_{\parallel} \approx (\tfrac{1}{2}) \tan^2 \Theta \tag{43}$$

The shape of non-Kramers' resonances is nonstandard in several respects. The inhomogeneous broadening appears to be related to a distribution in the intradoublet splitting Δ, in its turn possibly induced by a distribution in rhombicities (*168;* see also Refs. *162* and *169* and references quoted therein). As a result of the transition probability being proportional to the splitting Δ, the line shape is asymmetrically tailing toward low field and has a zero intensity at the effective g value for axial symmetry (*2, 162, 166*). Furthermore, in biological systems the distribution in Δ is frequently such that the resonance line is broadened "into zero field," i.e., $\Delta > h\nu$, with partial loss of intensity (*162*). Finally, in normal-mode spectra the powder pattern is deformed as a consequence of the zero transition probability along the z axis. All these effects combined have the result that reading effective g values directly from the polycrystal spectrum is usually much less accurate than with Kramers' systems. In many cases g_{eff} determinations are only possible by spectral simulation techniques adapted for integer-spin systems (*144, 162*). Also, for the quantification of powder spectra from non-Kramers' systems the use of spectral simulations appears to be mandatory; on a more advanced level these simulations become involved and time consuming (*144*). The bottom line is that there is no quick and easy way to quantitate these spectra.

When discussing high-spin Kramers' systems we noted that for $S > \frac{3}{2}$ higher order terms in the spin operator should be added to the spin

Hamiltonian. We decided that this is very rarely done, possibly because second and higher order terms result in similar effects in the powder spectrum. This is not true for non-Kramers' systems. For example, for a rhombic $S = 2$ system the complete zero-field Hamiltonian is an extension of Eq. (30), namely (*2, 145, 170, 171*):

$$\begin{aligned} H_{ZF} = {} & (a/6)[S_x^4 + S_y^4 + S_z^4 - (\tfrac{1}{5})S(S+1)(3S^2 + 3S - 1)] \\ & + (F/180)[35S_z^4 - 30S(S+1)S_z^2 \\ & + 25S_z^2 - 6S(S+1) + 3S^2(S+1)^2] \\ & + D[S_z^2 - S(S+1)/3] + E[S_x^2 - S_y^2) \\ & + (b/2)\{[7S_z^2 - S(S+1) - 5](S_x^2 - S_y^2) \\ & + (S_x^2 - S_y^2)[7S_z^2 - S(S+1) - 5]\} \end{aligned} \tag{44}$$

When we calculate the approximate values for the non-Kramers' doublet splittings under this Hamiltonian (they are given in Fig. 10), it can be seen that the effects of the new a, F, and b terms are easily incorporated, by substitution, into the old D and E terms, except for a splitting of the second doublet linear in the quantity a. This has the far-reaching implication that the upper doublet can be split even in cubic symmetry, therefore that no rhombicity is required for a finite transition probability. We have made one attempt at rigorously analyzing a bimodal spectrum ($S = 2$ in cytochrome oxidase) with the Hamiltonian of Eq. (44), and we have found the a term to dominate the splitting of the second doublet (*144*). It would appear that all studies on biological non-Kramers' doublets ignoring this term are incomplete.

B. Iron–Sulfur Non-Kramers' Systems

EPR on non-Kramers' systems was introduced to the field of iron-sulfur clusters with the detection of an $S = 2$ signal from the $[3Fe–4S]^0$ cluster in the 7Fe *Thermus thermophilus* ferredoxin (*107*). The spectra (see Fig. 11) were very similar to those previously found for $S = 2$ in other biological and model systems (*162*). Only a single, asymmetric feature is observed extending toward zero field such that the main intensity of the first-derivative spectrum is below the base line. The line is assigned to the transition within the second doublet, subject to a broad distribution in Δ_2. The transition is $|\Delta m| = 0$, but is generally referred to as "$|\Delta m| = 4$" (*105, 107, 144, 162*) to indicate that it originates from the second non-Kramers' doublet, for which the high-field labeling is $|\pm 2\rangle$. Figure 11 also shows the main effect of raising the

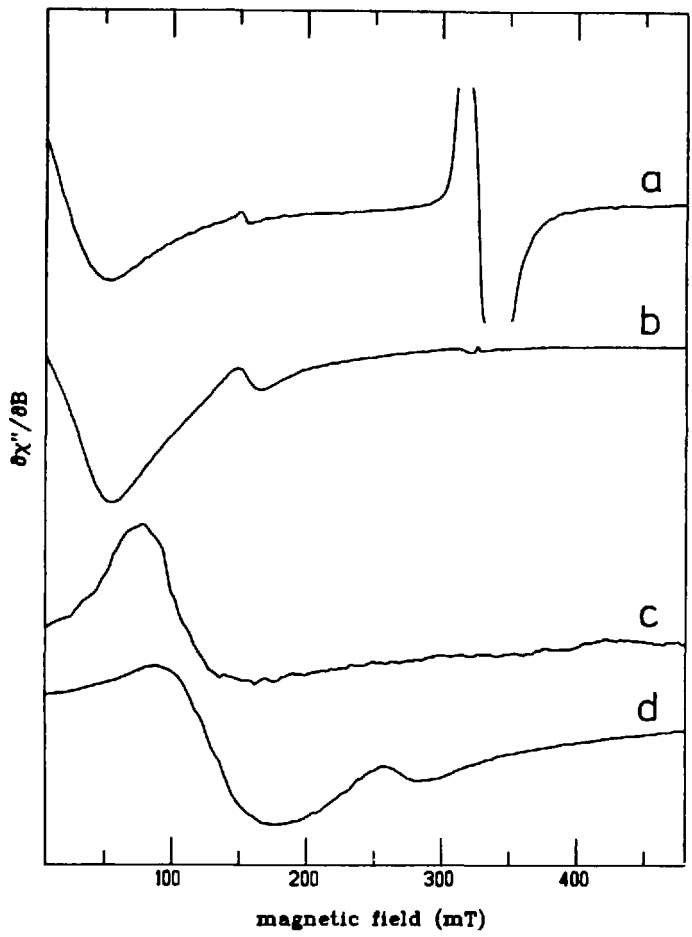

FIG. 11. The $S = 2$ X-band EPR from the $[3Fe–4S]^0$ cluster in *Thermus thermophilus* ferredoxin (trace a) and ferrous EDTA (trace b), and their respective P-band spectra (traces c and d). The $S = \frac{1}{2}$ signal around $g = 2$ in trace (a) is from the oxidized [3Fe–4S] cluster (*107*).

magnitude of the microwave quantum. The spectral feature at higher frequency has a less asymmetric shape due to the fact that a smaller fraction of the distributed Δ values disappears into zero field.

The 7Fe ferredoxin contains a [3Fe–4S] and a [4Fe–4S] cluster at a mutual distance of the order of $\approx$1 nm (*45*, *46*). This is the typical distance for which dipole–dipole interactions show up in the EPR spectrum as broadenings, shifts, and/or splittings. The 7Fe ferredoxins have

a protein fold similar to the 8Fe ferredoxins (*45, 46*). The latter contain two [4Fe–4S] cubanes, and in the reduced state show EPR spectra with dipole–dipole effects between two $S = \frac{1}{2}$ spins (*172*). The reduced 7Fe ferredoxin is special in that the interaction is between $S = \frac{1}{2}$ (the cubane) and $S = 2$. The $S = 2$ EPR (cf. Fig. 11) is too broad to detect dipolar effects, however, the cubane spectrum *is* affected in an unusual way: the interaction signal has some effective g values that are constant in the microwave frequency. This effect appears to be a direct consequence of the non-Kramers' nature of the disturbing spin (*107*).

A signal similar to that of Fig. 11 has been observed for the $[3Fe–4S]^0$ cluster in *D. gigas* ferredoxin II (*105*), probably for the *D. gigas* Ni–Fe hydrogenase (*173*), and possibly also for aconitase (quoted in Ref. *169*).

The determination of zero-field splitting parameters for non-Kramers' systems is more difficult than for Kramers' systems. The ambiguity introduced by the extra terms in the spin Hamiltonian, Eq. (44), especially the a term (cf. Fig. 10), makes it impossible to read a rhombicity directly from the spectrum. Unambiguous assignment requires the detection of resonances from *both* non-Kramers' doublets of an $S = 2$ system (*144*). This notion is still not generally appreciated (*105, 169*). Also, the determination of the intradoublet splitting in terms of the dominant D quantity [or its effective substitute in accordance with Eq. (44), $D' \approx D + 2F/15 + a/5$] is apparently not trivial. For the *T. thermophilus* ferredoxin, a positive D was indicated by EPR, whereas MCD spectroscopy clearly indicated a negative D (*107*). It was then suggested that the EPR was complicated by relaxation phenomena (*107*). Except for an early, naive attempt by the present author (*162*), spin lattice relaxation in biological non-Kramers' systems has not been explored.

We have very recently identified two new iron–sulfur non-Kramers' systems (*57, 59*). The EPR differs from that of hitherto reported biological $S = 2$ systems in two respects: (1) the line width is reduced by an order of magnitude and (2) the ratio of parallel-mode over normal-mode intensity has increased by an order of magnitude compared to the ratio of ≈ 2, predicted by Eq. (43) and thus far found in practice (cf. Ref. *169*). The bimodal spectrum for one of the systems is given in Fig. 12. The signal is from an intermediate redox state of the putative iron–sulfur supercluster, the P-cluster in the *A. vinelandii* Mo–Fe nitrogenase. The effective g value is ≈ 12, and this is unusual because thus far determined—by spectral simulation—g_{eff} values for biological non-Kramers' systems are usually close to 8 (*162*). Note that some previously reported (cf. Refs. *173–175*) g values close to 12 are only *apparent* values corresponding to the zero crossing of the asymmetrical spec-

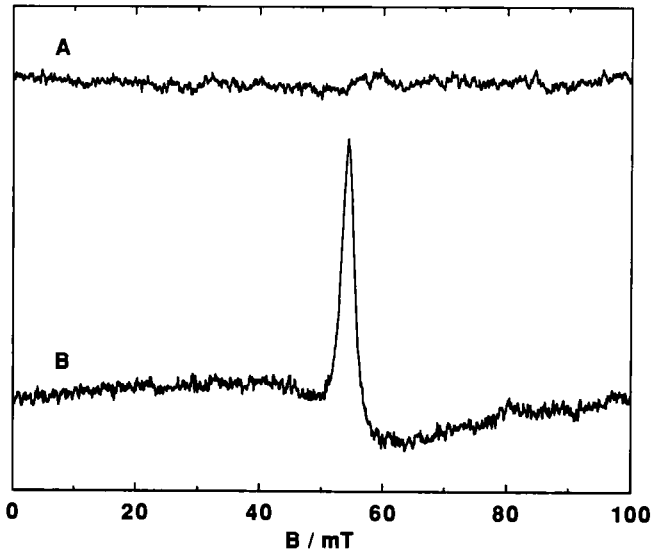

FIG. 12. Dual-mode $S = 3$ X-band EPR from the P-cluster in *Azobacter vinelandii* nitrogenase Mo–Fe protein poised at a potential of −188 mV at pH 7.5. Trace A is the normal-mode spectrum, i.e., with B perpendicular to B_1; trace B is the parallel-mode spectrum, i.e., with B parallel to B_1. The two spectra were taken with the same bimodal cavity, all conditions, other than the frequency mode, being identical (*57*).

tral feature of the "$|\Delta m| = 4$" transition at X-band. These values have no physical meaning.

A simple model to explain the spectrum of Fig. 12 is to assume that the system is $S = 3$, and the resonance is from the highest doublet, i.e., "$|\Delta m| = 6$" with $g_{\text{eff}} = 12$ (*57*). No serious attempts have been made yet to support this view with simulations based on the $S = 3$ equivalent of the spin Hamiltonian in Eq. (44) (which should now also encompass sixth-order terms in S, i.e., of the form S^6).

The second novel system is the putative prismane protein, which in one of its intermediate redox states exhibits a sharp parallel-mode signal with $g_{\text{eff}} \approx 16$ (*59*). By the same token, this signal is identified with a "$|\Delta m| = 8$" transition within the highest doublet of an $S = 4$ system (*59*).

These intuitive interpretations may perhaps soon prove to be premature. They do, however, make it clear that in the field of iron–sulfur EPR there is a considerable need for theoretical development regarding non-Kramers' spins and superspins.

VI. Epilogue

EPR spectroscopy of iron–sulfur complexes and proteins is in its fourth decade. It was suggested in Section I that the field is experiencing its third renaissance; the body of this article gives support to this view. In conjunction with the opening up of the area of superclusters we expect to see important developments in our understanding of high-spin EPR, both for half-integer and integer systems. Data on these novel clusters and on the well-characterized "classical" two-, three-, and four-iron clusters will inspire us to further assess the relevance of mechanisms of double-exchange interactions. Also, it is hoped that work on the g-strain concept will gain impetus as new experimental data become available. Because of these progressions the iron–sulfur protein has by far long outdone the hemoprotein as the pet object of those interested in the development of metalloprotein EPR.

For various reasons, certain subjects have not explicitly been treated in this article. The mechanisms used by the $[2Fe–2S]^{1+}$ cluster for spin lattice relaxation have been shown to be standard (*176*), and with no other data available we have nothing to add but to assume that this is true also for other clusters. Similarly, the mixed-metal clusters were not a separate theme. The Mo–Fe and V–Fe clusters in nitrogenases were referred to for their $S = \frac{3}{2}$ EPR; however, the Co-, Zn-, and Cd-substituted cubanes (*154, 177, 178*) and a putative W–Fe–S cluster (*179*) were not treated, as there appears to be nothing fundamentally new in their EPR properties. The EPR-related double-resonance and pulsed techniques were left out partly because of limitations of size, but also because recent reviews of metalloproteins are available (*180, 181*).

One subject, that of the mixed spins, was swept under the rug because of a complete lack of theorization on its physical and biochemical nature. In recent times it has become increasingly evident that many iron–sulfur systems exist as a mixture of two or more spin states. This has been found for cubane structures (*83, 84, 91, 125, 126, 151, 160, 182–184*) and for superclusters (*51, 52, 56, 57, 59*). The term "physical mixture" has been proposed (*184*) to indicate that these states appear not to mix thermodynamically or quantum mechanically. One would hope that it will not take until the next renaissance of iron–sulfur EPR before it will dawn on us what a physical mixture of spin states means.

ACKNOWLEDGMENTS

S. P. J. Albracht introduced me to the Fe–S field some 15 years ago, and he continues to help me with the bimodal EPR. W. R. Dunham taught me the QM and a lot more; he

is now a key collaborator on the supercluster project. A. J. Pierik did most of the recent superspin EPR for his PhD thesis; he also made some of the figures for this article. I have had invaluable support from R. H. Sands and from C. Veeger. Support is acknowledged from the Netherlands Foundation for Chemical Research (SON), with financial aid from the Netherlands Organization for Scientific Research (NWO).

REFERENCES

1. Zavoisky, E., *Fiz. Zh.* **9,** 211 (1945).
2. Abragam, A., and Bleaney, B., "Electron Paramagnetic Resonance of Transition Ions." Oxford Univ. Press (Clarendon), Oxford, 1970.
3. Bennett, J. E., Ingram, D. J. E., George, P., and Griffith, J. S., *Nature (London)* **176,** 394 (1955).
4. Bennett, J. E., and Ingram, D. J. E., *Nature (London)* **177,** 275 (1956).
5. Sands, R. H., *Phys. Rev.* **99,** 1222 (1955).
6. Sands, R. H., and Beinert, H., *Biochem. Biophys. Res. Commun.* **1,** 175 (1959).
7. Beinert, H., and Sands, R. H., *Biochem. Biophys. Res. Commun.* **3,** 41 (1960).
8. Sands, R. H., and Beinert, H., *Biochem. Biophys. Res. Commun.* **3,** 47 (1960).
9. Blumberg, W. E., and Peisach, J., *in* "Non-Heme Iron Proteins: Role in Energy Conservation" (A. San Pietro, ed.), p. 101. Antioch Press, Yellow Springs, Ohio, 1965.
10. Brintzinger, H., Palmer, G., and Sands, R. H., *Proc. Natl. Acad. Sci. U.S.A.* **55,** 397 (1966).
11. Van Voorst, J. D. W., and Hemmerich, P., *in* "Magnetic Resonance in Biological Systems" (A. Ehrenberg, B. G. Malmström, and T. Vänngård, eds.), p. 183. Pergamon, Oxford, 1967.
12. Johnson, C. E., Bray, R. C., Cammack, R., and Hall, D. O., *Proc. Natl. Acad. Sci. U.S.A.* **63,** 1234 (1969).
13. Gibson, J. F., Hall, D. O., Thornley, J. H. M., and Whatley, F. R., *Proc. Natl. Acad. Sci. U.S.A.* **56,** 987 (1966).
14. Thornley, J. H. M., Gibson, J. F., Whatley, F. R., and Hall, D. O., *Biochem. Biophys. Res. Commun.* **24,** 877 (1966).
15. Palmer, G., Dunham, W. R., Fee, J. A., Sands, R. H., Iizuka, T., and Yonetani, T., *Biochim. Biophys. Acta* **245,** 201 (1971).
16. Fritz, J., Anderson, R., Fee, J., Palmer, G., Sands, R. H., Tsibris, J. C. M., Gunsalus, I. C., Orme-Johnson, W. H., and Beinert, H., *Biochim. Biophys. Acta* **253,** 110 (1971).
17. Dunham, W. R., Bearden, A. J., Salmeen, I. T., Palmer, G., Sands, R. H., Orme-Johnson, W. H., and Beinert, H., *Biochim. Biophys. Acta* **253,** 134 (1971).
18. Eaton, W., Palmer, G., Fee, J. A., Kimura, T., and Lovenberg, W., *Proc. Natl. Acad. Sci. U.S.A.* **68,** 3015 (1971).
19. Dunham, W. R., Palmer, G., Sands, R. H., and Bearden, A. J., *Biochim. Biophys. Acta* **253,** 373 (1971).
20. Bertrand, P., and Gayda, J.-P., *Biochim. Biophys. Acta* **597,** 107 (1979).
21. Bertrand, P., and Gayda, J.-P., *Biochim. Biophys. Acta* **625,** 337 (1980).
22. Gayda, J.-P., Bertrand, P., More, C., and Cammack, R., *Biochimie* **63,** 847 (1981).
23. Bertrand, P., Guigliarelli, B., Gayda, J.-P., Bearwood, P., and Gibson, J. F., *Biochim. Biophys. Acta* **831,** 261 (1985).
24. Guigliarelli, B., Bertrand, P., and Gayda, J.-P., *J. Chem. Phys.* **85,** 1689 (1986).

25. Hearshen, D. O., Hagen, W. R., Sands, R. H., Grande, H. J., Crespi, H. L., Gunsalus, I. C., and Dunham, W. R., *J. Magn. Reson.* **69,** 440 (1986).
26. Emptage, M. H., *Am. Chem. Soc. Symp. Ser.* **372,** 343 (1988).
27. Beinert, H., and Kennedy, M. C., *Eur. J. Biochem.* **186,** 5 (1989).
28. Switzer, R. L., *BioFactors* **2,** 77 (1989).
29. Orme-Johnson, N. R., Orme-Johnson, W. H., Hansen, R. E., Beinert, H., and Hatefi, Y., *Biochem. Biophys. Res. Commun.* **44,** 446 (1971).
30. DerVartanian, D. V., Morgan, T. V., and Brantner, R. V., *Biochim. Biophys. Acta* **347,** 497 (1974).
31. Forget, P., and DerVartanian, D. V., *Biochim. Biophys. Acta* **256,** 600 (1972).
32. Beinert, H., Ackrell, B. A. C., Kearney, E. B., and Singer, T. P., *Biochem. Biophys. Res. Commun.* **58,** 564 (1974).
33. Ruzicka, F. J., and Beinert, H., *Biochem. Biophys. Res. Commun.* **58,** 556 (1974).
34. Ruzicka, F. J., and Beinert, H., *J. Biol. Chem.* **253,** 2514 (1978).
35. Sweeney, W. V., Rabinowitz, J. C., and Yoch, D. C., *J. Biol. Chem.* **250,** 7842 (1975).
36. Beinert, H., *in* "Iron-Sulfur Proteins" (W. Lovenberg, ed.), Vol. 3, p. 84. Academic Press, New York, 1977.
37. Emptage, M. H., Kent, T. A., Huynh, B. H., Rawlings, J., Orme-Johnson, W. H., and Münck, E., *J. Biol. Chem.* **255,** 1793 (1980).
38. Beinert, H., and Thomson, A. J., *Arch. Biochem. Biophys.* **222,** 333 (1983).
39. Beinert, H., Emptage, M. H., Dreyer, J.-L., Scott, R. A., Hahn, J. E., Hodgson, K. O., and Thomson, A. J., *Proc. Natl. Acad. Sci. U.S.A.* **80,** 393 (1983).
40. Kent, T. A., Dreyer, J.-L., Kennedy, M. C., Huynh, B. H., Emptage, M. H., Beinert, H., and Münck, E., *Proc. Natl. Acad. Sci. U.S.A.* **79,** 1096 (1982).
41. Kennedy, M. C., Kent, T. A., Emptage, M. H., Merkle, H., Beinert, H., and Münck, E., *J. Biol. Chem.* **259,** 14463 (1984).
42. Emptage, M. H., Kent, T. A., Kennedy, M. C., Beinert, H., and Münck, E., *Proc. Natl. Acad. Sci. U.S.A.* **80,** 4674 (1983).
43. Kent, T. A., Emptage, M. H., Merkle, H., Kennedy, M. C., Beinert, H., and Münck, E., *J. Biol. Chem.* **260,** 6871 (1985).
44. Stout, C. D., Ghosh, D., Patthabi, B., and Robbins, A. H., *J. Biol. Chem.* **255,** 1797 (1980).
45. Stout, G. H., Turley, S., Sieker, L. C., and Jensen, L. H., *Proc. Natl. Acad. Sci. U.S.A.* **85,** 1020 (1988).
46. Stout, C. D., *J. Biol. Chem.* **263,** 9256 (1988).
47. Kanatzidis, M. G., Hagen, W. R., Dunham, W. R., Lester, R. K., and Coucouvanis, D., *J. Am. Chem. Soc.* **107,** 953 (1985).
48. Hagen, W. R., van Berkel-Arts, A., Krüse-Wolters, K. M., Voordouw, G., and Veeger, C., *FEBS Lett.* **203,** 59 (1986).
49. Hagen, W. R., Wassink, H., Eady, R. R., Smith, B. E., and Haaker, H., *Eur. J. Biochem.* **169,** 457 (1987).
50. Hagen, W. R., Pierik, A. J., and Veeger, C., *J. Chem. Soc., Faraday Trans. 1* **85,** 4083 (1989).
51. Pierik, A. J., Hagen, W. R., and Veeger, C., *EBEC Rep.* **6,** 16 (1990).
52. Hagen, W. R., Pierik, A. J., and Veeger, C., *Ital. Biochem. Soc. Trans.* **1,** 85 (1990).
53. Jetten, M. S. M., Hagen, W. R., Pierik, A. J., Stams, A. J. M., and Zehnder, A. J. B., *Eur. J. Biochem.* **195,** 385 (1991).
54. Pierik, A. J., and Hagen, W. R., *Eur. J. Biochem.* **195,** 505 (1991).
55. Hagen, W. R., Pierik, A. J., Wolbert, R. B. G., Wassink, H., Haaker, H., Veeger, C.,

Jetten, M. K., Stams, A. J. M., and Zehnder, A. J. B., *J. Inorg. Biochem.* **43,** 237 (1991).
56. Jetten, M. S. M., Pierik, A. J., and Hagen, W. R., *Eur. J. Biochem.* **202,** 1291 (1991).
57. Pierik, A. J., Wassink, H., Haaker, H., and Hagen, W. R., *Eur. J. Biochem.* (submitted for publication).
58. Pierik, A. J., Wolbert, R. B. G., Hagen, W. R., and Veeger, C., *Eur. J. Biochem.* (submitted for publication).
59. Pierik, A. J., Hagen, W. R., Dunham, W. R., and Sands, R. H., *Eur. J. Biochem.* (submitted for publication).
60. Adams, M. W. W., Eccleston, E., and Howard, J. B., *Proc. Natl. Acad. Sci. U.S.A.* **86,** 4932 (1989).
61. George, G. N., Prince, R. C., Stokley, K. E., and Adams, M. W. W., *Biochem. J.* **259,** 597 (1989).
62. Adams, M. W. W., *Biochim. Biophys. Acta* **1020,** 115 (1990).
63. Ravi, N., Moura, I., Tavares, P., LeGall, J., Huynh, B. H., and Moura, J. J. G., *J. Inorg. Biochem.* **43,** 252 (1991).
64. Bolin, J. T., Ronco, A. E., Mortenson, L. E., Morgan, T. V., Williamson, M., and Xuong, N.-H., *in* "Nitrogen Fixation: Achievements and Objectives" (P. M. Gresshoff, L. E. Roth, G. Stacey, and W. E. Newton, eds.), p. 117. Chapman & Hall, New York, 1990.
65. Bolin, J. T., Campobasso, N., Muchmore, S. W., Minor, W., Mortenson, L. E., and Morgan, T. V., *J. Inorg. Biochem.* **43,** 447 (1991).
66. Nomenclature Committee of the International Union of Biochemistry. Recommendations 1978, *Biochim. Biophys. Acta* **549,** 101 (1979); Recommendations 1989, *Eur. J. Biochem.* **200,** 599 (1991).
67. Orme-Johnson, W. H., and Sands, R. H., *in* "Iron-Sulfur Proteins" (W. Lovenberg, ed.), Vol. 2, Chap. 5. Academic Press, New York, 1973.
68. Orme-Johnson, W. H., and Orme-Johnson, N. R., *in* "Iron-Sulfur Proteins" (T. G. Spiro, ed.), Chap. 2. Wiley, New York, 1982.
69. Moura, I., Macedo, A., and Moura, J. J. G., *in* "Advanced EPR. Applications in Biology and Biochemistry" (A. J. Hoff, ed.), Chap. 23. Elsevier, Amsterdam, 1989.
70. Eaton, W. A., and Lovenberg, W., *in* "Iron-Sulfur Proteins" (W. Lovenberg, ed.), Vol. 2, p. 131. Academic Press, New York, 1973.
71. Hagen, W. R., *Eur. J. Biochem.* **182,** 523 (1989).
72. Moura, I., Xavier, A. V., Cammack, R., Bruschi, M., and LeGall, J., *Biochim. Biophys. Acta* **533,** 156 (1978).
73. Tavares, P., Ravi, N., Liu, M. Y., LeGall, J., Huynh, B. H., Moura, J. J. G., and Moura, I., *J. Inorg. Chem.* **43,** 264 (1991).
74. LeGall, J., Prickril, B. C., Moura, I., Xavier, A. V., Moura, J. J. G., and Huynh, B.-H., *Biochemistry* **27,** 1636 (1988).
75. Maltempo, M. M., and Moss, T. H., *Q. Rev. Biophys.* **9,** 181 (1976).
76. Palmer, G., and Brintzinger, H., *Nature (London)* **211,** 189 (1966).
77. Moura, I., Tavares, P., Moura, J. J. G., Ravi, N., Huynh, B. H., Liu, M.-Y., and LeGall, J., *J. Biol. Chem.* **265,** 21596 (1990).
78. Yost, F. J., and Fridovich, I., *J. Biol. Chem.* **248,** 4905 (1973).
79. Coucouvanis, D., Salisoglou, A., Kanatzidis, M. G., Dunham, W. R., Simopoulos, A., and Kostikas, A., *Inorg. Chem.* **27,** 4066 (1988).
80. Weigel, J. A., Holm, R. H., Surerus, K. K., and Münck, E., *J. Am. Chem. Soc.* **111,** 9246 (1989).
81. Norland, B., Sjöberg, V. B. M., and Eklund, H., *Nature (London)* **345,** 593 (1990).

82. Orme-Johnson, W. H., Hansen, R. E., Beinert, H., Tsibris, J. C. M., Bartolomaus, R. C., and Gunsalus, I. C., *Proc. Natl. Acad. Sci. U.S.A.* **60,** 368 (1968).
83. Moulis, J.-M., Auric, P., Gaillard, J., and Meyer, J., *J. Biol. Chem.* **259,** 11396 (1984).
84. Gaillard, J., Moulis, J.-M., Auric, P., and Meyer, J., *Biochemistry* **25,** 464 (1986).
85. Cline, J. F., Hoffman, B. M., Mims, W. B., LaHaie, E., Ballou, D. P., and Fee, J. A., *J. Biol. Chem.* **260,** 3251 (1985).
86. Telser, J., Hoffman, B. M., LoBrutto, R., Ohnishi, T., Tsai, A. L., Simpkin, D., and Palmer, G., *FEBS Lett.* **214,** 117 (1987).
87. Gurbiel, R. J., Batie, C. J., Sivaraja, M., True, A. E., Fee, J. A., Hoffman, B. M., and Ballou, D. P., *Biochemistry* **28,** 4861 (1989).
88. Britt, R. D., Sauer, K., Klein, M. P., Knaff, D. B., Kriauciunas, A., Yu, C.-A., Yu, L., and Malkin, R., *Biochemistry* **30,** 1892 (1991).
89. George, S. J., Armstrong, F. A., Hatchikian, E. C., and Thomson, A. J., *Biochem. J.* **264,** 275 (1989).
90. Armstrong, F. A., *Struct. Bonding* **72,** 137 (1990).
91. Conover, R. C., Kowal, A. T., Fu, W., Park, J.-B., Aono, S., Adams, M. W. W., and Johnson, M. K., *J. Biol. Chem.* **265,** 8533 (1990).
92. Münck, E., Debrunner, P. G., Tsibris, J. C. M., and Gunsalus, I. C., *Biochemistry* **11,** 855 (1972).
92. Hille, R., Hagen, W. R., and Dunham, W. R., *J. Biol. Chem.* **260,** 10569 (1985).
94. Varret, F., *J. Phys. (Paris)* **37,** C6, 437 (1976).
95. Coffman, R. E., and Stavens, B. W., *Biochem. Biophys. Res. Commun.* **41,** 163 (1970).
96. Tsukihara, T., Fukuyama, K., Tahara, H., Katsube, Y., Matsuura, Y., Tanaka, N., Kakudo, M., Wada, K., and Matsubara, H., *J. Biochem. (Tokyo)* **84,** 1645 (1978).
97. Hearshen, D. O., Dunham, W. R., Sands, R. H., and Grande, H. J., *in* "Electron Transport and Oxygen Utilization" (C. Ho, ed.), p. 395. Elsevier, New York, 1982.
98. Noodleman, L., and Baerends, E. J., *J. Am. Chem. Soc.* **106,** 2316 (1984).
99. Anderson, P. W., and Hasegawa, H., *Phys. Rev.* **100,** 675 (1955).
100. Middleton, P., Dickson, D. P. E., Johnson, C. E., and Rush, J. D., *Eur. J. Biochem.* **88,** 135 (1978).
101. Day, E. P., Peterson, J., Bonvoisin, J. J., Moura, I., and Moura, J. J. G., *J. Biol. Chem.* **263,** 3684 (1988).
102. Snyder, B. S., Patterson, G. S., Abrahamson, A. J., and Holm, R. H., *J. Am. Chem. Soc.* **111,** 5214 (1989).
103. Surerus, K. K., Münck, E., Snyder, B. S., and Holm, R. H., *J. Am. Chem. Soc.* **111,** 5501 (1989).
104. Ding, X.-Q., Bominaar, E. L., Bill, E., Winkler, H., Trautwein, A. X., Drüeke, S., Chaudhuri, P., and Wieghart, K., *J. Chem. Phys.* **92,** 178 (1990).
105. Papaefthymiou, V., Girerd, J.-J., Moura, I., Moura, J. J. G., and Münck, E., *J. Am. Chem. Soc.* **109,** 4703 (1987).
106. Münck, E., and Kent, T. A., *Hyperfine Interact.* **27,** 161 (1986).
107. Hagen, W. R., Dunham, W. R., Johnson, M. K., and Fee, J. A., *Biochim. Biophys. Acta* **828,** 369 (1985).
108. Sands, R. H., and Dunham, W. R., *Q. Rev. Biophys.* **7,** 443 (1975).
109. Girerd, J.-J., Papaefthymiou, V., Surerus, K. K., and Münck, E., *Pure Appl. Chem.* **61,** 805 (1989).
110. Kent, T. A., Huynh, B. H., and Münck, E., *Proc. Natl. Acad. Sci. U.S.A.* **77,** 6574 (1980).

111. Gayda, J. P., Bertrand, P., Theodule, F.-X., and Moura, J. J. G., *J. Chem. Phys.* **77,** 3387 (1982).
112. Münck, E., *in* "Iron–Sulfur Proteins" (T. G. Spiro, ed.), Chap. 4. Wiley, New York, 1982.
113. Gayda, J. P., Bertrand, P., Guigliarelli, B., and Meyer, J., *J. Chem. Phys.* **79,** 5732 (1983).
114. Bertrand, P., Guigliarelli, B., Meyer, J., and Gayda, J. P., *Biochimie* **66,** 43 (1984).
115. Guigliarelli, B., Gayda, J. P., Bertrand, J., and More, C., *Biochim. Biophys. Acta* **871,** 149 (1986).
116. Guigliarelli, B., More, C., Bertrand, P., and Gayda, J. P., *J. Chem. Phys.* **85,** 2774 (1986).
117. Evans, M. C. W., Hall, D. O., and Johnson, C. E., *Biochem. J.* **119,** 289 (1970).
118. Dickson, D. P. E., Johnson, C. E., Cammack, R., Evans, M. C. W., Hall, D. O., and Rao, K. K., *Biochem. J.* **139,** 105 (1974).
119. Middleton, P., Dickson, D. P. E., Johnson, C. E., and Rush, J. D., *Eur. J. Biochem.* **104,** 289 (1980).
120. Noodleman, L., *Inorg. Chem.* **27,** 3677 (1988).
121. Jordanov, J., Roth, E. K. H., Fries, P. H., and Noodleman, L., *Inorg. Chem.* **29,** 4288 (1990).
122. Banci, L., Bertini, I., and Luchinat, C., *Struct. Bonding* **72,** 113 (1990).
123. Lucinat, C., *J. Inorg. Biochem.* **43,** 239 (1991).
124. Antanaitis, B. C., and Moss, T. H., *Biochim. Biophys. Acta* **405,** 262 (1975).
125. Dunham, W. R., Hagen, W. R., Fee, J. A., Sands, R. H., Dunbar, J. B., and Humblet, C., *Biochim. Biophys. Acta* **1079,** 253 (1991).
126. Hagen, W. R., *in* "Advanced EPR. Applications in Biology and Biochemistry" (A. J. Hoff, ed.), Chap. 22. Elsevier, Amsterdam, 1989.
127. Beinert, H., and Albracht, S. P. J., *Biochim. Biophys. Acta* **683,** 245 (1982).
128. Aasa, R., and Vänngård, T., *J. Magn. Reson.* **19,** 308 (1975).
129. Isomoto, A., Watari, H., and Kotani, M., *J. Phys. Soc. Jpn.* **29,** 1571 (1970).
130. Johnston, T. S., and Hecht, H. G., *J. Mol. Spectrosc.* **17,** 98 (1965).
131. Venable, J. H., *in* "Magnetic Resonance in Biological Systems" (A. Ehrenberg, B. G. Malmström, and T. Vänngård, eds.), p. 373. Pergamon, Oxford, 1967.
132. Hagen, W. R., and Albracht, S. P. J., *Biochim. Biophys. Acta* **702,** 61 (1982).
133. Guigliarelli, B., Gayda, J.-P., Bertrand, P., and More, C., *Biochim. Biophys. Acta* **871,** 149 (1986).
134. Hagen, W. R., *J. Magn. Reson.* **44,** 447 (1981).
135. Strong, L. H., Ph.D. Thesis, The University of Michigan, Ann Arbor, Michigan (1976).
136. Hagen, W. R., Hearshen, D. O., Sands, R. H., and Dunham, W. R., *J. Magn. Reson.* **61,** 220 (1985).
137. Hearshen, D. O., Ph.D. Thesis, The University of Michigan, Ann Arbor, Michigan (1983).
138. Hagen, W. R., *in* "Cytochrome Systems. Molecular Biology and Bioenergetics" (S. Papa, B. Chance, and L. Ernster, eds.), p. 459. Plenum, New York, 1987.
139. Hagen, W. R., Hearshen, D. O., Harding, L. J., and Dunham, W. R., *J. Magn. Reson.* **61,** 233 (1985).
140. Salerno, J. C., and Siedow, J. N., *Biochim. Biophys. Acta* **579,** 246 (1979).
141. Cockle, S., Lindskog, S., and Grell, E., *Biochem. J.* **143,** 703 (1974).
142. Pake, G. E., and Estle, T. L., "The Physical Principles of Electron Paramagnetic Resonance," 2nd Ed., Chap. 4. Benjamin, Reading, Massachusetts, 1973.

143. Oosterhuis, W. T., *Struct. Bonding* **20,** 59 (1974).
144. Hagen, W. R., Dunham, W. R., Sands, R. H., Shaw, R. W., and Beinert, H., *Biochim. Biophys. Acta* **765,** 399 (1984).
145. Von Waldkirch, Th., Müller, K. A., and Berlinger, W. *Phys. Rev. B* **5,** 4324 (1972).
146. Troup, G. J., and Hutton, D. R., *Br. J. Appl. Phys.* **15,** 1493 (1964).
147. Blumberg, W. E., *in* "Magnetic Resonance in Biological Systems" (A. Ehrenberg, B. G. Malmström, and T. Vänngård, eds.), p. 119. Pergamon, Oxford, 1967.
148. Münck, E., Rhodes, H., Orme-Johnson, W. H., Davis, L. C., Brill, W. J., and Shah, V. K., *Biochim. Biophys. Acta* **400,** 32 (1975).
149. Hagen, W. R., *in* "Cytochrome Systems. Molecular Biology and Bioenergetics" (S. Papa, B. Chance, and L. Ernster, eds.), p. 459. Plenum, New York, 1987.
150. Morningstar, J. E., and Hales, B. J., *J. Am. Chem. Soc.* **109,** 6854 (1987).
151. Lindahl, P. A., Day, E. P., Kent, T. A., Orme-Johnson, W. H., and Münck, E., *J. Biol. Chem.* **260,** 11160 (1985).
152. Hagen, W. R., 1991. The DOS-program "RHOMBO" computes effective g-values for $S = \frac{3}{2}$ through $\frac{9}{2}$ as a function of rhombicity and real g-value. Available freely upon request.
153. Rawlings, J., Shah, V. K., Chisnell, J. R., Brill, W. R., Zimmermann, R., Münck, E., and Orme-Johnson, W. H., *J. Biol. Chem.* **253,** 1001 (1978).
154. Surerus, K., Münck, E., Moura, I., Moura, J. J. G., and LeGall, J., *J. Am. Chem. Soc.* **109,** 3805 (1987).
155. Verhagen, M. F. J. M., and Hagen, W. R., unpublished results, 1991.
156. Smith, B. E., Lowe, D. J., and Bray, R. C., *Biochem. J.* **130,** 641 (1972).
157. Zimmermann, R., Münck, E., Brill, W. J., Shah, V. K., Henzl, M. T., Rawlings, J., and Orme-Johnson, W. H., *Biochim. Biophys. Acta* **537,** 185 (1978).
158. Watt, G. D., Burns, A., Laough, S., and Tennent, D. L., *Biochemistry* **21,** 4926 (1980).
159. Johnson, M. K., Thomson, A. J., Robinson, A. E., and Smith, B. E., *Biochim. Biophys. Acta* **671,** 61 (1981).
160. Hagen, W. R., Eady, R. R., Dunham, W. R., and Haaker, H., *FEBS Lett.* **189,** 250 (1985).
161. Zambrano, I. C., Kowal, A. T., Mortenson, L. E., Adams, M. W. W., and Johnson, M. K., *J. Biol. Chem.* **264,** 20974 (1989).
162. Hagen, W. R., *Biochim. Biophys. Acta* **708,** 82 (1982).
163. Aasa, R., *J. Chem. Phys.* **52,** 3919 (1970).
164. Dunham, W. R., Hagen, W. R. L., Braaksma, A., Haaker, H., Gheller, S., Newton, W. E., and Smith, B., *in* "Nitrogen Fixation Research Progress" (H. J. Evans, P. J. Bottomley, and W. E. Newton, eds.), p. 591. Martinus Nijhoff, Dordrecht, The Netherlands, 1985.
165. Bleaney, B., and Scovil, H. E. D., *Philos. Mag.* **43,** 999 (1952).
166. Baker, J. M., and Bleaney, B., *Proc. R. Soc. London A* **245,** 156 (1958).
167. De Groot, M. S., and van der Waals, J. H., *Mol. Phys.* **3,** 190 (1960).
168. Bleaney, B., Llewellyn, P. M., Price, M. H. L., and Hall, G. R., *Philos. Mag.* **45,** 991 (1954).
169. Hendrich, M. P., and Debrunner, P. G., *Biophys. J.* **56,** 489 (1989).
170. Jabłoński, R., Krukowska-Fulde, B., and Niemyski, T., *Mater. Res. Bull.* **8,** 53 (1973).
171. Jabłoński, R., Domańska, M., Krukowska-Fulde, B., and Niemyski, T., *Mater. Res. Bull.* **8,** 749 (1973).
172. Mathews, R., Charlton, S., Sands, R. H., and Palmer, G., *J. Biol. Chem.* **249,** 4326 (1974).

173. LeGall, J., Ljungdahl, P. O., Moura, I., Peck, H. D., Xavier, A. V., Moura, J. J. G., Teixera, M., Huynh, B. H., and DerVartanian, D. V., *Biochem. Biophys. Res. Commun.* **106,** 610 (1982).
174. Greenaway, F. T., Chan, S. H. P., and Vincow, G., *Biochim. Biophys. Acta* **490,** 62 (1977).
175. Brudvig, G. W., Stevens, T. H., Morse, R. H., and Chan, S. I., *Biochemistry* **20,** 3912 (1981).
176. Gayda, J.-P., Bertrand, P., Deville, A., More, C., Roger, G., Gibson, J. F., and Cammack, R., *Biochim. Biophys. Acta* **581,** 15 (1979).
177. Moura, I., Moura, J. J. G., Münck, E., Papaefthymiou, V., and LeGall, J., *J. Am. Chem. Soc.* **108,** 349 (1986).
178. Butt, J., Armstrong, F. A., Breton, J., George, S. J., Thomson, A. J., and Hatchikian, E. C., *J. Am. Chem. Soc.* **113,** 6663 (1991).
179. Mukund, S., and Adams, M. W. W., *J. Biol. Chem.* **265,** 11508 (1990).
180. Hoffman, B. M., Gurbiel, R. J., Werst, M. M., and Sivaraja, M., *in* "Advanced EPR. Applications in Biology and Biochemistry" (A. J. Hoff, ed.), Chap. 14. Elsevier, Amsterdam, 1989.
181. Mims, W. B., and Peisach, J., *in* "Advanced EPR. Applications in Biology and Biochemistry" (A. J. Hoff, ed.), Chap. 1. Elsevier, Amsterdam, 1989.
182. Watt, G. D., and McDonald, J. W., *Biochemistry* **24,** 7226 (1985).
183. Lindahl, P. A., Gorelick, N. J., Münck, E., and Orme-Johnson, W. H., *J. Biol. Chem.* **262,** 14945 (1987).
184. Carney, M. J., Papaefthymiou, G. C., Spartalian, K., Frankel, R. B., and Holm, R. H., *J. Am. Chem. Soc.* **110,** 6084 (1988).